J|A|C|S
ARTICLES
Published on Web 10/03/2002

Catalyst/Cocatalyst Nuclearity Effects in Single-Site Polymerization. Enhanced Polyethylene Branching and α-Olefin Comonomer Enchainment in Polymerizations Mediated by Binuclear Catalysts and Cocatalysts via a New Enchainment Pathway

Liting Li,[†] Matthew V. Metz,[†] Hongbo Li,[†] Ming-Chou Chen,[†] Tobin J. Marks,*[,†] Louise Liable-Sands,[‡] and Arnold L. Rheingold[‡]

Contribution from the Department of Chemistry, Northwestern University, Evanston, Illinois 60208-3113, and the Department of Chemistry and Biochemistry, University of Delaware, Newark, Delaware 19716-2522

Received February 1, 2002

Abstract: The binuclear "constrained geometry catalyst" (CGC) (μ-CH_2CH_2-3,3′){(η^5-indenyl)[1-Me_2Si-(^{t}BuN)]($ZrMe_2$)}$_2$ [EBICGC($ZrMe_2$)$_2$; **Zr$_2$**] and the trityl bisborate dianion (Ph_3C^+)$_2$[1,4-(C_6F_5)$_3$BC_6F_4B(C_6F_5)$_3$]$^{2-}$ (**B$_2$**) have been synthesized to serve as new types of multicenter homogeneous olefin polymerization catalysts and cocatalysts, respectively. Additionally, the complex [1-Me_2Si(3-ethylindenyl)(^{t}BuN)]$ZrMe_2$ (**Zr$_1$**) was synthesized as a mononuclear control. For the bimetallic catalyst or bisborate cocatalyst, high effective local active site concentrations and catalyst center−catalyst center cooperative effects are evidenced by bringing the catalytic centers together via either covalent or electrostatic bonding. For ethylene homopolymerization at constant conversion, the branch content of the polyolefin products (primarily ethyl branches) is dramatically increased as catalyst or cocatalyst nuclearity is increased. Moreover, catalyst and cocatalyst nuclearity effects are approximately additive. Compared to the catalyst derived from monometallic **Zr$_1$** and monofunctional $Ph_3C^+B(C_6F_5)_4^-$ (**B$_1$**), the active catalyst derived from bimetallic **Zr$_2$** and bifunctional **B$_2$** produces ∼11 times more ethyl branches in ethylene homopolymerization via a process which is predominantly intradimer in character. Moreover, ∼3 times more 1-hexene incorporation in ethylene + 1-hexene copolymerization and ∼4 times more 1-pentene incorporation in ethylene + 1-pentene copolymerization are observed for **Zr$_2$** + **B$_2$** versus **Zr$_1$** + **B$_1$**.

Introduction

In optimum scenarios for enzymatic catalysis, complex and dynamic multicenter active site−substrate interactions poise reacting functional groups in close, conformationally advantageous spacial proximities.[1] Among other effects, such cooperativity achieves high effective reagent local concentrations and consequently enhanced reactivity and selectivity by bringing reactants together via physical or chemical means. Beyond what is understood about such effects in vivo, several impressive in vitro systems have also been demonstrated.[1] Considerable evidence also supports the importance of metal center−metal center cooperative effects in a variety of metalloenzyme-catalyzed processes.[2] In this regard, polymetallic complexes having two or more transition-metal centers have been intensively investigated with the ultimate, increasingly successful goal of achieving unique catalytic transformations arising from cooperative reactivity effects between multiple metal centers.[3,4] Despite this effort, few possibilities have been explored in the rapidly advancing and technologically important field of homogeneous single-site olefin polymerization,[5] and those binuclear metallocenium catalysts studied to date have exhibited few noteworthy cooperativity characteristics other than somewhat depressed polymerization activities and broadened product polydispersities.[6,7] In typical exploratory homogeneous olefin

* Address correspondence to this author. E-mail: t-marks@northwestern.edu.
[†] Northwestern University.
[‡] University of Delaware.

(1) (a) Bruice, T. C.; Benkovic, S. J. *Biochemistry* **2000**, *39*, 6267−6274 and references therein. (b) O'Brien, D. P.; Entress, R. M. N.; Matthew, A. C.; O'Brien, S. W.; Hopkinson, A.; Williams, D. H. *J. Am. Chem. Soc.* **1999**, *121*, 5259−5265. (c) Carazo-Salas, R. E.; Guarguaglini, G.; Gruss, O. J.; Segref, A.; Karsenti, E.; Mattaj, L. W. *Nature* **1999**, *400*, 178−181. (d) Chiu, C. C.; Chung, A.; Barletta, G.; Jordan F. *J. Am. Chem. Soc.* **1996**, *118*, 11026−111029. (e) Menger, F. M. *Acc. Chem. Res.* **1993**, *26*, 206−212 and references therein. (f) Menger, F. M.; Venkataram, U. V. *J. Am. Chem. Soc.* **1985**, *107*, 4706−4709. (g) Page, M. I. In *The Chemistry of Enzyme Action*; Page, M. I., Ed.; Elsevier: New York, 1984, pp 1−54.

(2) (a) Steinhagen, H.; Helmchen, G. *Angew Chem., Int. Ed. Engl.* **1996**, *35*, 2339−2342. (b) Wilcox, D. E. *Chem. Rev.* **1996**, *96*, 2435−2458. (c) Sträter, N.; Lipscomb, W. N.; Klabunde, T.; Krebs, B. *Angew. Chem., Int. Ed. Engl.* **1996**, *35*, 2024−2055.

(3) Examples of systems without direct metal−metal bonds: (a) Jacobsen, E. N. *Acc. Chem. Res.* **2000**, *33*, 421−431 and references therein. (b) Molenveld, P.; Engbersen, J. F. J.; Reinhoudt, D. N. *Chem. Soc. Rev.* **2000**, *29*, 75−86. (c) Konsler, R. G.; Karl, J.; Jacobsen, E. N. *J. Am. Chem. Soc.* **1998**, *120*, 10780−10781. (d) Molenveld, P.; Kapsabelis, S.; Engbersen, J. F. J.; Reinhoudt, D. N. *J. Am. Chem. Soc.* **1997**, *119*, 2948−2949. (e) Mathews, R. C.; Howell, D. H.; Peng, W.-J.; Train, S. G.; Treleaven, W. D.; Stanley, G. G. *Angew. Chem., Int. Ed. Engl.* **1996**, *35*, 2253−2256. (f) Sawamura, M.; Sudoh, M.; Ito, Y. *J. Am. Chem. Soc.* **1996**, *118*, 3309−3310. (g) Broussard, M. E.; Juma, B.; Train, S. G.; Peng, W.-J.; Laneman, S.; Stanley, G. G. *Science* **1993**, *260*, 1784−1788.

polymerization experiments or in large-scale production facilities, catalyst concentrations are typically very low ($10^{-4}-10^{-8}$ M). This raises the intriguing question of whether appropriately designed bimetallic structures having two *sterically open* active centers in close proximity might provide high local catalyst concentrations and hence exhibit enhanced selectivity for distinctive enchainment pathways, including those which normally require sequential intermolecular process at two different metal centers. Possible consequences could include the possibility of synthesizing polymeric products having significantly altered microstructures.

Group 4 "constrained geometry catalysts" (CGC) are well-known single-site polymerization catalysts[8] that produce branched polyethylenes under conditions in which vinyl-terminated, chain-transferred macromolecules enjoy a significant probability of competitive reinsertion into the growing polymer chain at a second (remote) catalyst center (Scheme 1). The resulting small but significant levels of long-chain branching lead to highly desirable materials properties.[8] The intriguing question then arises whether if two CGC catalyst centers could be held in sufficiently close spacial proximity and in proper mutual orientations, an eliminated, olefin-terminated fragment might have an enhanced probability of being captured/enchained by a proximate active center before diffusing away. The possibility of cooperative effects between the two metal centers might likewise have a significant influence on the course of olefinic copolymerizations. Such nuclearity effects would be of both fundamental scientific and technological interest if new, more efficient ways to enhance comonomer incorporation and chain branching could be discovered.

Scheme 1. Mechanism for Long Chain Branch Formation in Ethylene Homopolymerization Mediated by Constrained Geometry Catalysts

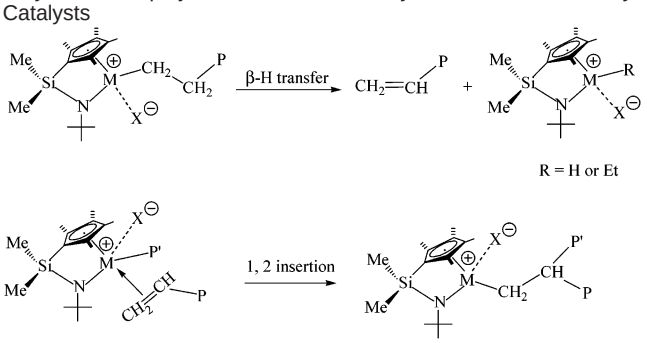

CGC Catalyst M = Ti, Zr, Hf; X^- = Cocatalyst-Derived Weakly-Coordinating Anion; P, P' = Alkyl/Polyolefin Chain.

Scheme 2. Catalyst−Cocatalyst Nuclearity Matrix

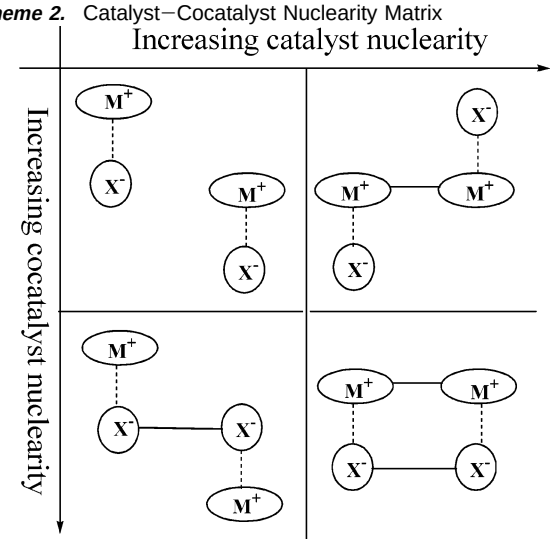

Two means (covalent and electrostatic) of bringing single-site polymerization catalyst centers into close proximity are illustrated in the nuclearity matrix of Scheme 2. We report[9] here the synthesis, characterization, and comparative ethylene homopolymerization characteristics of all four members of such a series—prepared from the new bimetallic "constrained geometry" catalyst (CGC), M = zirconium complex (μ-CH_2CH_2-3,3′){(η^5-indenyl)[1- Me_2Si(^{t}BuN)]($ZrMe_2$)}$_2$ [EBICGC($ZrMe_2$)$_2$] (**Zr$_2$**), the monometallic analogue [1-Me_2Si(3-ethylindenyl)-(^{t}BuN)]$ZrMe_2$ (**Zr$_1$**) for control experiments, as well as the new binuclear bisborate cocatalyst (Ph_3C^+)$_2$[1,4-(C_6F_5)$_3$BC_6F_4B-(C_6F_5)$_3$]$^{2-}$ (**B$_2$**),[10] and $Ph_3C^+B(C_6F_5)_4^-$ (**B$_1$**). The ethylene + 1-hexene and ethylene + 1-pentene copolymerization charac-

(4) Systems with direct metal−metal bonds: (a) Fukuoka, A.; Fukagawa, S.; Hirano, M.; Koga, N.; Komiya, S. *Organometallics* **2001**, *20*, 2065−2075. (b) Fulton, J. R.; Hanna, T. A.; Bergman, R. G. *Organometallics* **2000**, *19*, 602−614. (c) Fabre, S.; Findeis, G.; Trosch, J. M.; Gade, L. H.; Scowen, I. J.; McPartlin, M. *Chem. Commun*. **1999**, 577−578. (d) Schubart, M.; Mitchell, G.; Gade, L. H.; Kottke, T.; Scowen, I. J.; McPartlin, M. *Chem. Commun*. **1999**, 233−234. (e) *Catalysis by Di- and Polynuclear Metal Cluster Complexes*; Adams, R. D., Cotton, F. A., Eds.; Wiley-VCH: New York, 1998; see also references therein. (f) Schneider, A.; Gade, L. H.; Breuning, M.; Bringmann, G.; Scowen, I. J.; McPartlin, M. *Organometallics* **1998**, *17*, 1643−1645. (g) Misumi, Y.; Ishii, Y.; Hidai, M. *J. Chem. Soc., Dalton Trans.* **1995**, 3489−3496 (h) Adams, R. D.; Barnard, T. S.; Lu, Z.; Wu, W.; Yamamoto, J. H. *J. Am. Chem. Soc.* **1994**, *116*, 9103−9113.

(5) For recent reviews of single-site olefin polymerization, see (a) Pedeutour, J.-N.; Radhakrishnan, K.; Cramail, H.; Deffieux, A. *Macromol. Rapid Commun.* **2001**, *22*, 1095−1123. (b) Gladysz, J. A., Ed.; *Chem. Rev.* **2000**, *100* (special issue on "Frontiers in Metal-Catalyzed Polymerization"). (c) Marks, T. J.; Stevens, J. C., Eds.; *Topics Catal*. **1999**, *15*, and references therein. (d) Britovsek, G. J. P.; Gibson, V. C.; Wass, D. F. *Angew. Chem., Int. Ed.* **1999**, *38*, 428−447. (e) Kaminsky, W.; Arndt, M. *Adv. Polym. Sci.* **1997**, *127*, 144−187. (f) Bochmann, M. *J. Chem. Soc., Dalton Trans.* **1996**, 255−270. (g) Brintzinger, H.-H.; Fischer, D.; Mülhaupt, R.; Rieger, B.; Waymouth, R. M. *Angew. Chem., Int. Ed. Engl*. **1995**, *34*, 1143−1170. (h) *Catalyst Design for Tailor-Made Polyolefins*; Soga, K., Terano, M., Eds.; Elsevier: Tokyo, 1994. (i) Möhring, P. C.; Coville, N. J. *J. Organomet. Chem.* **1994**, *479*, 1−29. (j) Marks, T. J. *Acc. Chem. Res.* **1992**, *25*, 57−65.

(6) For polymerization studies with binuclear metallocenes, see ref 7 and (a) Spaleck, W.; Küber, F.; Bachmann, B.; Fritze, C.; Winter, A. *J. Mol. Catal. A: Chem.* **1998**, *128*, 279−287. (b) Yan, X.; Chernega, A.; Green, M. L. H.; Sanders, J.; Souter, J.; Ushioda, T. *J. Mol. Catal. A: Chem.* **1998**, *128*, 119−141. (c) Soga, K.; Ban, H. T.; Uozumi, T. *J. Mol. Catal. A: Chem.* **1998**, *128*, 273−278. (d) Bochmann, M.; Cuenca, T.; Hardy, D. T. *J. Organomet. Chem.* **1994**, *484*, C10−C12. (e) Jungling, S.; Mülhaupt, R.; Plenio, H. *J. Organomet. Chem.* **1993**, *460*, 191−195.

(7) (a) Lee, D. H.; Yoon, K. B.; Lee, E. H.; Noh, S. K.; Byun, G. G.; Lee, C. S. *Macromol. Rapid Commun.* **1995**, *16*, 265−268. (b) Lee, D. H.; Yoon, K. B.; Noh, S. K.; Kim, S. C.; Huh, W. S. *Macromol. Rapid Commun.* **1995**, *16*, 265−268. (c) Noh, S. K.; Byun, G. G.; Lee, C. S.; Lee, D. H.; Yoon, K. B.; Kang, K. S. *J. Organomet. Chem.* **1996**, *518*, 1−6. (d) Noh, S. K.; Kim, J. M.; Jung, J. H.; Ra, C. S.; Lee, D. H.; Lee, H. B.; Lee, S. W.; Huh, W. S. *J. Organomet. Chem.* **1999**, *580*, 90−97. (e) Noh, S. K.; Kim, S. C.; Kim, J. H.; Lee, D. H.; Yoon, K. B.; Lee, H. B.; Lee, S. W.; Huh, W. S. *J. Polym. Sci., Part A: Polym. Chem.* **1997**, *35*, 3717−3728.

(8) (a) Chum, P. S.; Kruper, W. J.; Guest, M. J. *Adv. Mater*. **2000**, *12*, 1759−1767. (b) Alt, H. G.; Föttinger, K.; Milius, W. *J. Organomet. Chem.* **1999**, 572, 21−30. (c) Harrison, D.; Coulter, I. M.; Wang, S. T.; Nistala, S.; Kuntz, B. A.; Pigeon, M.; Tian, J.; Collins, S. *J. Mol. Catal. A: Chem.* **1998**, *128*, 65−77. (d) Nesarikar, A. R.; Carr, S. H.; Khait, K.; Mirabella, F. M. *J. Appl. Polym. Sci.* **1997**, *63*, 1179−1187. (e) Soga, K.; Uozumi, T.; Nakamura, S.; Toneri, T.; Teranishi, T.; Sano, T.; Arai, T.; Shiono, T. *Macromol. Chem. Phys.* **1996**, *197*, 4237−4251. (f) Devore, D. D.; Timmers, F. J.; Hasha, D. L.; Rosen, R. K.; Marks, T. J.; Deck, P. A.; Stern, C. L. *Organometallics* **1995**, *14*, 3132−3134. (g) Stevens, J. C. *Proc. MetCon Houston*, **1993**, 157. (h) Lai, S. Y.; Wilson, J. R.; Knight, G. W.; Stevens, J. C. WO-93/08221, 1993. (i) Canich, J. M.; Hlatky, G. G.; Turner, H. W. *PCT Appl*. WO 92-00333, 1992; Canich, J. M. *Eur. Patent Appl*. EP 420 436-A1, 1991 (Exxon Chemical Co.) (j) Devore, D. D. Eur. Pat. Appl. EP-514-828-A1, Nov 25, 1992. (k) Stevens, J. C.; Timmers, F. J.; Wilson, D. R.; Schmidt, G. F.; Nickias, P. N.; Rosen, R. K.; Knight, G. W.; Lai, S. Eur. Pat. Appl. EP 416 815-A2, 1991 (Dow Chemical Co.).

(9) For a preliminary communication of certain parts of this work, see (a) Li, L.; Metz, M. V.; Marks, T. J.; Liable-Sands, L.; Rheingold, A. *Polymer Preprints*, **2000**, *41*, 1912−1913. (b) Patton, J. T.; Marks, T. J.; Li, L. *WO9914222A1*, March 25, 1999.

teristics with the four combinations of metallocene catalysts and borate cocatalysts illustrated in the catalyst nuclearity matrix (Scheme 2) are also examined. It will be seen that the effect of increasing catalyst and cocatalyst nuclearity is to dramatically enhance certain polyethylene chain branching architectures in

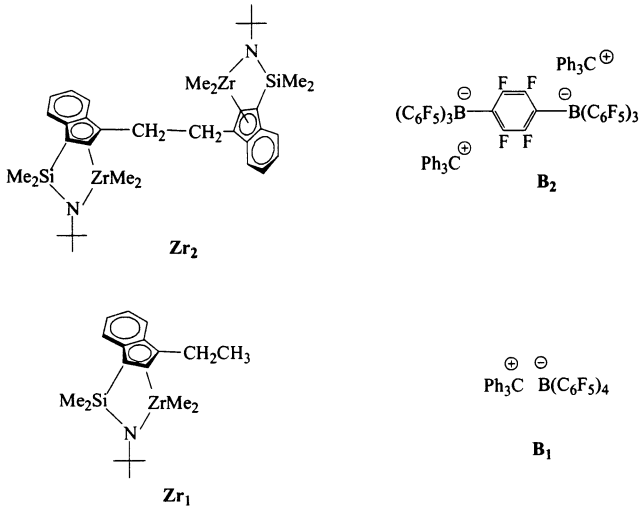

the homopolymerization process as well as α-olefin comonomer enchainment in α-olefin copolymerizations via a mechanism involving the first identified cooperative effects between single-site polymerization centers.

Results

The goal of this study was to investigate the possibility and nature of cooperative effects between two proximate single-site active catalytic centers, exploring potential enhancement of polyethylene chain branching in ethylene homopolymerization and, on the basis of that result, α-olefin incorporation in ethylene + α-olefin copolymerizations. Coordinatively "open" and highly reactive CGC core structures[8] are employed. For initial studies, Zr-based CGC complexes were chosen since these are known to produce relatively low molecular mass polyethylenes which are readily amenable to detailed microstructural characterization by ^{1}H and ^{13}C NMR spectroscopy. Thus, new bimetallic catalyst **Zr$_2$**, monometallic catalyst **Zr$_1$**, and binuclear bisborate cocatalyst $(Ph_3C^+)_2[1,4\text{-}(C_6F_5)_3BC_6F_4B(C_6F_5)_3]^{2-}$ (**B$_2$**) were synthesized for this purpose. The four combinations of metallocene catalysts and borate cocatalysts illustrated in Scheme 2 were then employed in ethylene homopolymerization studies. For reasons to be discussed below, the results of the homopolymerization experiments prompted parallel studies of ethylene + 1-hexene, ethylene + 1-pentene, and ethylene + 1-pentene-d_5 copolymerizations. It will be seen that the effect of increasing catalyst and cocatalyst nuclearity is to significantly enhance polyethylene chain branching (predominantly ethyl) in the homopolymerization process and α-olefin comonomer incorporation in the copolymerizations.

(10) Other bifunctional borane and borate cocatalysts have been recently reported: (a) Metz, M. V.; Schwartz, D. J.; Stern, C. L.; Nickias, P. N.; Marks, T. J. *Organometallics*, in press. (b) Metz, M. V.; Schwartz, D. J.; Stern, C. L.; Nickias, P. N.; Marks, T. J. *Angew. Chem., Int. Ed.* **2000**, *39*, 1312−1316. (c) McAdon, M. H.; Nickias, P. N.; Marks, T. J.; Schwartz, D. J. *WO9906413A1*, Feb 11, 1999. (d) Williams, V. C.; Piers, W. E.; Clegg, W.; Elsegood, M. R. J.; Collins, S.; Marder, T. B. *J. Am. Chem. Soc.* **1999**, *121*, 3244−3245.

Scheme 3. Synthesis of Linked Binuclear Indenyl Constrained Geometry Ligand

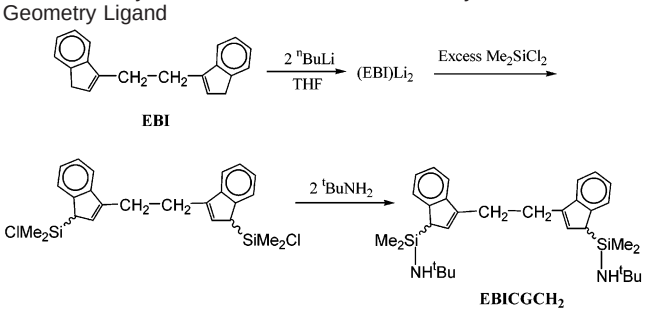

Scheme 4. Synthesis of Binuclear Indenyl Constrained Geometry Complexes

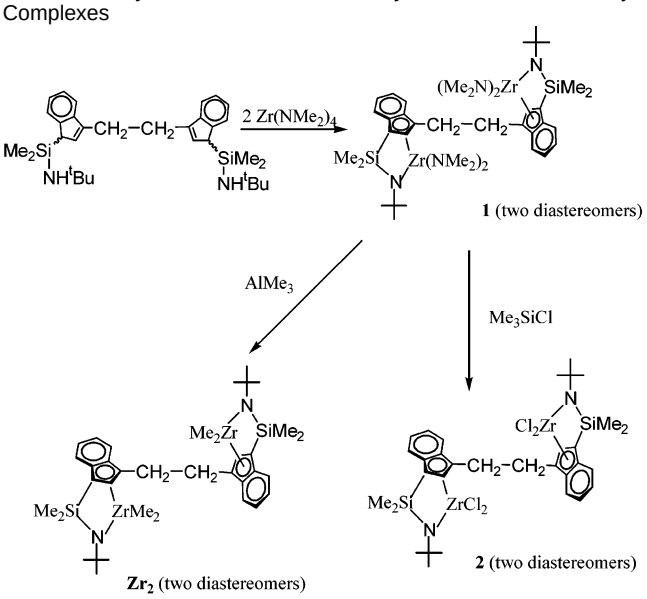

I. Synthesis of Bimetallic Complex EBICGC(ZrMe$_2$)$_2$ (Zr$_2$). The binuclear ligand synthesis is reasonably straightforward and is illustrated in Scheme 3. Excess Me_2SiCl_2 is employed in reaction with $(EBI)Li_2$ to prepare (μ-CH_2CH_2-3,3′)[1-(Me_2SiCl)indenyl]$_2$ which is produced in two diastereomers [(*RR*, *SS*) and (*RS*, *SR*)] in an approximately 1:1 ratio as assessed by ^{1}H and ^{13}C NMR spectroscopy. The two isomers have slightly different solubilities in pentane, and one isomer can be isolated in a pure state. The reaction of (μ-CH_2CH_2-3,3′)[1-(Me_2SiCl)indenyl]$_2$ with excess ^{t}BuNH$_2$ cleanly forms the desired ligand (μ-CH_2CH_2-3,3′)[1-(Me_2SiNH^tBu)Indenyl]$_2$ (EBICGCH$_2$) which also consists of two diastereomers, (*RR*, *SS*) and (*RS*, *SR*), in an approximately 1:1 ratio as indicated by ^{1}H and ^{13}C NMR spectra.

Bimetallic precatalyst complex EBICGC(ZrMe$_2$)$_2$ (**Zr$_2$**) was synthesized via the protodeamination methodology outlined in Scheme 4. The first step is the synthesis of bimetallic amido complex EBICGC[Zr(NMe$_2$)$_2$]$_2$ (**1**) via reaction of the free ligand (μ-CH_2CH_2-3,3′)[1-(Me_2SiNH^tBu)indenyl]$_2$ (EBICGCH$_2$) with Zr(NMe$_2$)$_4$ in refluxing toluene with constant removal of byproduct $HNMe_2$.[11] The product consists of two diastereomers (*RS*, *SR*) and (*SS*, *RR*) (1:1.3 or 1.3:1 ratio) as indicated by ^{1}H NMR spectroscopy. Both diastereomers have low solubility in toluene and benzene and are virtually insoluble in pentane.

(11) A similar approach to mononuclear CGC complexes using M(NMe$_2$)$_4$ reagents (M = Ti, Zr, Hf) has been previously reported: Carpenetti, D. W.; Kloppenburg, L.; Kupec, J. T.; Petersen, J. L. *Organometallics* **1996**, *15*, 1572−1581.

Scheme 5. Synthesis of 3-Ethylindenyl Constrained Geometry Ligand

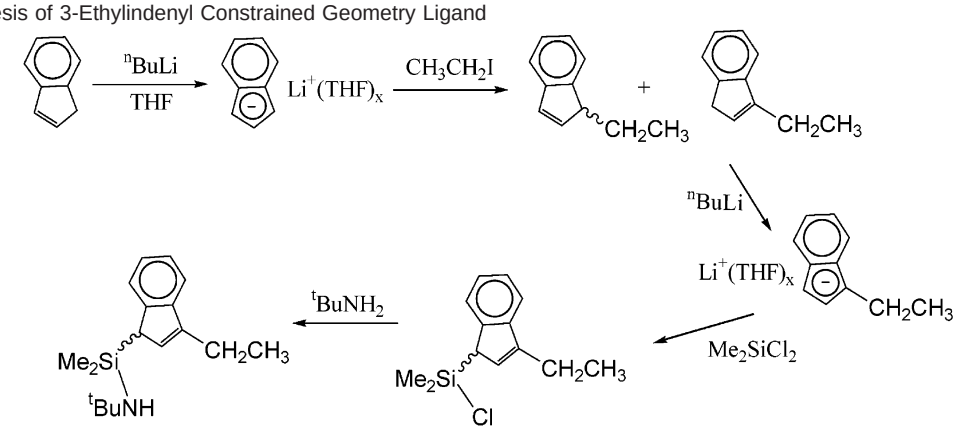

Attempts to isolate pure diastereomers by fractional crystallization were unsuccessful. Bimetallic amido complex **1** was characterized by standard spectroscopic and analytical techniques, and one diastereomer (*RS*, *SR*) by X-ray diffraction (vide infra). Reaction of **1** with excess $AlMe_3$ at room temperature cleanly forms bimetallic metallocene dimethyl complex **Zr$_2$**, which can be purified by repeatedly washing with pentane, and has been characterized spectroscopically and analytically. Both diastereomers (*RS*, *SR*) and (*SS*, *RR*) (1:1.3 or 1.3:1 ratio) are present in the product. The solubility of either diastereomer in toluene, benzene, and pentane is rather low, even at higher temperatures. Furthermore, the complexes begin to decompose above 80 °C in solution, which also complicates recrystallization. The reaction of EBICGC[$Zr(NMe_2)_2$]$_2$ (**1**) with excess Me_3SiCl affords EBICGC($ZrCl_2$)$_2$ (**2**) which has also been characterized by standard spectroscopic and analytical techniques. To our knowledge, complexes **1**, **2**, and **Zr$_2$** represent the first bimetallic CGC transition-metal complexes.

II. Synthesis of Monometallic Complex [1-Me$_2$Si(3-Ethylindenyl)(^{t}BuN)]ZrMe$_2$ (Zr$_1$). The monometallic complex [1-Me_2Si(3-ethylindenyl)(^{t}BuN)]$ZrMe_2$ (**Zr$_1$**) was synthesized for control experiments in studies of binuclear cooperativity effects. The ligand synthesis is illustrated in Scheme 5. The reagent 3-ethylindene is prepared via reaction of CH_3CH_2I with indenyllithium. The reagent 1-ethylindenyllithium, which is prepared in THF, undergoes further reaction with excess Me_2SiCl_2 to form the dimethyl(3-ethyl-1-indenyl)chlorosilane. After all the volatiles including unreacted Me_2SiCl_2 are removed in vacuo, the residue is dissolved in THF, and reaction with ^{t}BuNH$_2$ affords the desired ligand (1-Me_2SiNH^tBu)(3-ethyl)-indene. Monometallic CGC complex [1-Me_2Si(3-ethylindenyl)-(^{t}BuN)]$ZrMe_2$ (**Zr$_1$**) is synthesized via methodology similar to that for EBI(CGC$ZrMe_2$)$_2$ (**Zr$_2$**; Scheme 4). The monometallic amido complex [1-Me_2Si(3-ethylindenyl)(^{t}BuN)]Zr(NMe_2)$_2$ (**3**) is synthesized via the reaction of the free ligand (1-Me_2Si^t-BuNH)(3-ethyl)indene with $Zr(NMe_2)_4$ in refluxing toluene with constant removal of $HNMe_2$ (Scheme 6).[11] Reaction of **3** with excess Me_3SiCl at room temperature then cleanly affords dichloro complex [1-Me_2Si(3-ethylindenyl)(^{t}BuN)])]$ZrCl_2$ (**4**). Subsequent reaction with MeLi affords dimethyl complex [1-Me_2Si(3-ethylindenyl)(^{t}BuN)]$ZrMe_2$ (**Zr$_1$**). Complexes **4** and **Zr$_1$** were characterized by standard spectroscopic and analytical techniques and X-ray diffraction (vide infra).

III. Synthesis Binuclear Trityl Bis(tetrakisperfluroarylborate) Cocatalyst (Ph_3C^+)$_2$[1,4-(C_6F_5)$_3$BC_6F_4B(C_6F_5)$_3$]$^{2-}$(B$_2$). Binuclear trityl bisborate (Ph_3C^+)$_2$[1,4-(C_6F_5)$_3$BC_6F_4B(C_6F_5)$_3$]$^{2-}$

Scheme 6. Synthesis of Mononuclear Indenyl Constrained Geometry Complexes

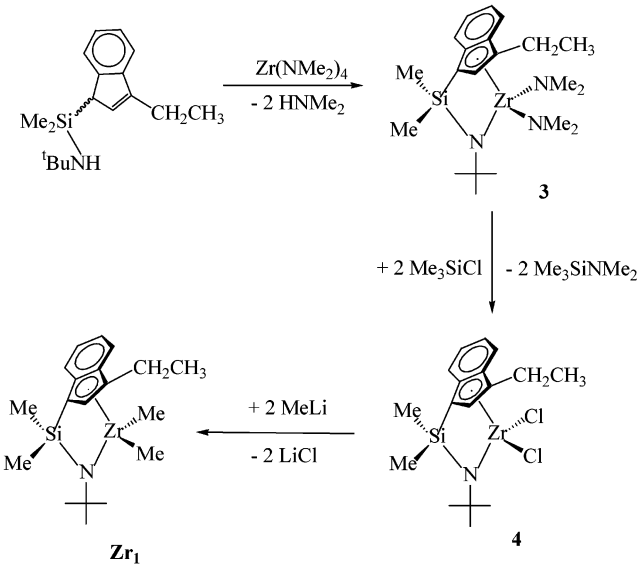

Scheme 7. Synthesis of Binuclear Bisperfluoroarylborate Cocatalyst

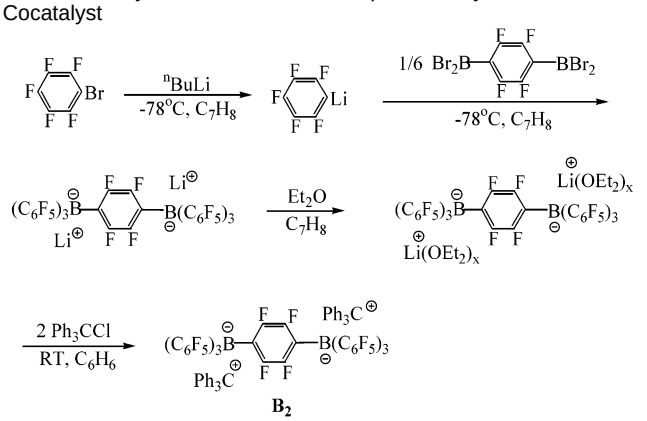

(**B$_2$**) was synthesized from bisborane 1,4-$Br_2BC_6F_4BBr_2$ (**5**), which in turn was prepared via reaction of 1,4- $Me_3SnC_6F_4$-$SnMe_3$[12] with neat BBr_3 (excess) for 2 days at room temperature (Scheme 7). The reagent 1,4-$Br_2BC_6F_4BBr_2$ (**5**) decomposes slowly at room temperature and must be stored at −20 °C. Reaction of bisborane **5** with 6 equiv of C_6F_5Li (generated in situ) affords bisborate dilithium salt (Li^+)$_2$[1,4-(C_6F_5)$_3$BC_6F_4B-(C_6F_5)$_3$]$^{2-}$. Et_2O is then added to yield (Li(OEt_2)x^+)$_2$[1,4-

(12) Chivers, T. *J. Organomet. Chem.* **1969**, *19*, 75−80.

Table 1. Summary of the Crystal Structure Data for Complexes **1**, **Zr_1**, and **4**

complex	**1**	**Zr_1**	**4**
formula	$C_{40}H_{68}N_6Si_2Zr_2$	$C_{19}H_{31}NSiZr$	$C_{17}H_{25}Cl_2NSiZr$
formula weight	871.62	392.76	433.59
crystal dimensions	0.50 × 0.35 × 0.15	0.20 × 0.31 × 0.17	0.20 × 0.17 × 0.21
crystal system	triclinic	monoclinic	monoclinic
a, Å	8.4173(2)	23.1827(15)	22.8427(19)
b, Å	9.9149(2)	12.2603(8)	12.1419(10)
c, Å	14.1349(3)	14.1942(9)	14.2712(12)
α, deg	83.2302(5)	90	90
β, deg	82.9329(7)	100.2350(10)	100.4390(10)
γ, deg	83.4330(2)	90	90
V, Å^3	1156.54(3)	3970.2(4)	3892.7(6)
space group	P1̄	*C*2/*c*	*C*2/*c*
Z value	2	8	8
D_{calc}, mg/m^3	1.251	1.314	1.480
temp *K*	198(2)	153(2)	153(2)
μ, cm^{-1}	5.34	6.12	6.97
radiation	MoK_α	MoK_α	MoK_α
2θ range, deg	1.46 to 28.04	1.79 to 28.27	1.81 to 28.29
no. of parameter	241	323	243
intensities (unique, R_i)	4907, 0.0416	4772, 0.0222	4678, 0.0190
R	0.0465	0.0356	0.0412
R^2w	0.1233	0.0797	0.1093

Table 2. Selected Bond Distances (Å) and Angles (deg) for EBICGC[Zr(NM_2)$_2$]$_2$ (**1**)

	Bond Distances		
Zr(1)−N(1)	2.133(2)	Zr(1)−N(2)	2.065(2)
Zr(1)−N(3)	2.049(2)	Zr(1)−C(1)	2.533(2)
Zr(1)−C(2)	2.491(2)	Zr(1)−C(3)	2.604(2)
Zr(1)−C(8)	2.673(2)	Zr(1)−C(9)	2.598(1)
N(1)−C(12)	1.496(3)	N(2)−C(16)	1.460(5)
Si(1)−C(2)	1.884(2)	Si(1)−N(1)	1.734(2)
	Angles		
N(3)−Zr(1)−N(2)	106.08(11)	N(3)−Zr(1)−N(1)	108.11(9)
N(2)−Zr(1)−N(1)	106.08(10)	N(1)−Si(1)−C(2)	95.67(10)
N(1)−Si(1)−C(11)	116.81(14)	C(2)−Si(1)−C(11)	108.18(13)
N(1)−Si(1)−C(10)	115.33(13)	C(12)−N(1)−Si(1)	127.6(2)
C(12)−N(1)−Zr(1)	126.6(2)	Si(1)−N(1)−Zr(1)	105.25(10)
C(16)−N(2)−C(17)	109.5(3)	C(16)−N(2)−Zr(1)	125.2(2)
C(17)−N(2)−Zr(1)	124.9(2)	C(18)−N(3)−C(19)	111.2(3)
C(18)−N(3)−Zr(1)	116.2(2)	C(19)−N(3)−Zr(1)	131.2(2)
C(1)−C(2)−C(3)	104.8(2)	C(1)−C(2)−Si(1)	120.6(2)
C(3)−C(2)−Si(1)	127.0(2)	C(1)−C(9)−C(8)	106.5(2)
C(1)−C(9)−C(20)	128.2(2)	C(8)−C(9)−C(20)	124.8(2)

$(C_6F_5)_3BC_6F_4B(C_6F_5)_3]^{2-}$, which undergoes subsequent cation metathesis with Ph_3CCl to afford bistrityl bisborate salt **B_2**. This new trityl bisborate was characterized by conventional spectroscopic and analytical methodologies.

IV. Molecular Structures of Complexes 1, Zr_1, and 4. A. Bimetallic Complex EBICGC[Zr(NMe_2)$_2$]$_2$ (1). A summary of crystal structure data for complex **1** is presented in Table 1. Selected bond distances and angles are summarized in Table 2. Figure 1A shows the solid-state structure of bimetallic bisdimethylamido complex **1**. The crystal structure contains an inversion center with a metallic CGC center located on either side of the ethylenebis(indenyl) fragment and with the two coordinated indenyl rings in a diastereomeric relationship. As can be seen from Figure 1A, the crystal consists of a single diastereomer (*SR*, *RS*). The sum of the bond angles around nitrogen atom N(1) is 359.45°, indicating atoms Si(1), N(1), C(12), and Zr(1) are essentially coplanar, which is also true for the atoms around dimethylamide atoms N(2) and N(3). Such coplanar structures suggest non-negligible π bonding between the Zr and N atoms involving the N atom lone pair electrons. The sum of bond angles around ring carbon atom C(2) is 352.4°,

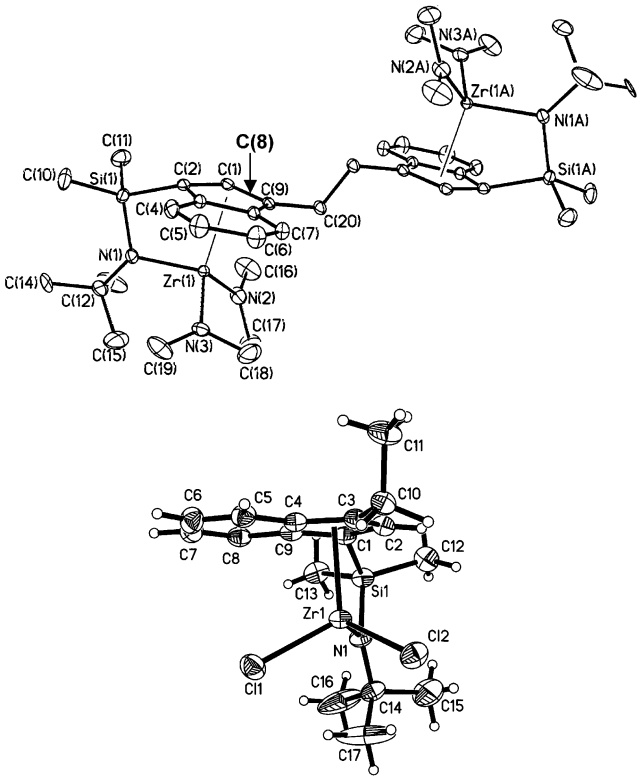

Figure 1. (A) Molecular structure and atom numbering scheme for bimetallic indenyl constrained geometry complex EBICGC[ZrNMe_2)$_2$]$_2$ (**1**). Thermal ellipsoids are drawn at the 30% probability level. A single enantiomer is shown. (B) Molecular structure and atom numbering scheme for monometallic indenyl constrained geometry complex [1-Me_2Si(3-ethylindenyl)(^{t}BuN)]ZrCl_2 (**4**). Thermal ellipsoids are drawn at the 50% probability level. A single enantiomer is shown.

indicating that the C(2)−Si(1) bond vector is displaced slightly from the ring plane because of the constrained geometry. As expected from previous structural results for analogous complexes, the carbon atoms of the Cp ring do not have equal bonding distances to the Zr center.[8,11] The Zr(1)−C(2) bond length (2.491(2) Å) is the shortest while the Zr(1)−C(8) bond length (2.673(2) Å) is the longest. The Me_2Si bridge induces a contraction in the indenyl(centroid)-Zr−N angle (105°) which renders the structure more open.

B. Monometallic Complexes 4 and Zr_1. A summary of crystal structure data for complexes **4** and **Zr_1** is given in Table 1, and selected bond distances and angles for **4** and **Zr_1** are summarized in Tables 3 and 4, respectively. The solid-state structures of **4** and **Zr_1** are illustrated in Figures 1B and 2, respectively. As expected, the metrical parameters in Tables 3 and 4 suggest that the Me_2Si bridge again forces the indenyl plane to tilt, which renders the structure coordinatively more open.[6] Similar to bimetallic complex **1**, the sum of the bond angles around bridge-connected nitrogen atom N(1) in both **4** and **Zr_1** is close to 360 °C, indicating the atoms around N(1) are essentially coplanar and suggesting strong Zr−N bonding, presumably involving π-donation. Because of the more electronegative character of the Cl ligands, the Zr center in **4** is more electron-deficient than that in **Zr_1**, leading to a significantly shorter Zr−N(1) bond length and significantly shorter Zr−C(ring) contacts in **4** than in **Zr_1**. Compared to bimetallic dimethylamido complex **1**, both the Zr−N(1) bond lengths and

Table 3. Selected Bond Distances (Å) and Angles (deg) for **4**

Bond Distances			
Zr(1)−N(1)	2.041(2)	Zr(1)−C(1)	2.409(2)
Zr(1)−Cl(2)	2.4292(7)	Zr(1)−Cl(1)	2.4366(8)
Zr(1)−C(2)	2.453(2)	Zr(1)−C(5)	2.506(2)
Zr(1)−C(3)	2.559(2)	Zr(1)−C(4)	2.597(2)
Si(1)−N(1)	1.750(2)	Si(1)−C(13)	1.859(3)
Si(1)−C(12)	1.863(3)	Si(1)−C(1)	1.871(2)
Angles			
N(1)−Zr(1)−Cl(2)	109.82(6)	N(1)−Zr(1)−Cl(1)	109.66(7)
Cl(2)−Zr(1)−Cl(1)	106.07(3)	N(1)−Si(1)−C(13)	115.21(13)
N(1)−Si(1)−C(12)	115.65(14)	C(14)−N(1)−Si(1)	128.27(17)
C(14)−N(1)−Zr(1)	125.80(16)	Si(1)−N(1)−Zr(1)	105.88(10)
C(2)−C(1)−C(5)	105.0(2)	C(2)−C(1)−Si(1)	121.27(19)
C(5)−C(1)−Si(1)	125.66(18)	C(2)−C(3)−C(4)	106.8(2)
C(2)−C(3)−C(10)	127.1(2)	C(4)−C(3)−C(10)	125.8(2)

Table 4. Selected Bond Distances (Å) and Angles (deg) for **Zr_1**

Bond Distances			
Zr(1)−N(1)	2.0664(15)	Zr(1)−C(19)	2.244(2)
Zr(1)−C(18)	2.256(2)	Zr(1)−C(2)	2.4279(17)
Zr(1)−C(3)	2.4744(17)	Zr(1)−C(1)	2.5318(17)
Zr(1)−C(4)	2.5881(17)	Zr(1)−C(5)	2.6297(17)
Si(1)−N(1)	1.7446(16)	Si(1)−C(13)	1.863(2)
Si(1)−C(12)	1.866(2)	Si(1)−C(2)	1.8767(18)
N(1)−C(14)	1.484(2)		
Angles			
N(1)−Zr(1)−C(19)	111.79(8)	N(1)−Zr(1)−C(18)	110.54(8)
C(19)−Zr(1)−C(18)	106.34(10)	N(1)−Si(1)−C(13)	115.36(10)
N(1)−Si(1)−C(12)	115.59(10)	C(13)−Si(1)−C(12)	107.78(11)
N(1)−Si(1)−C(2)	94.46(7)	C(14)−N(1)−Si(1)	129.29(12)
C(14)−N(1)−Zr(1)	125.69(12)	Si(1)−N(1)−Zr(1)	104.98(7)
C(3)−C(2)−C(1)	104.70(15)	C(3)−C(2)−Si(1)	121.28(13)
C(1)−C(2)−Si(1)	125.94(13)	C(3)−C(4)−C(5)	106.60(15)
C(3)−C(4)−C(10)	127.35(17)	C(5)−C(4)−C(10)	125.62(16)

Zr−C(ring) distances in **4** and **Zr_1** are significantly shorter because the Zr center in **1** is more electron-rich because of Zr−N π-bonding involving the dimethylamido nitrogen lone pairs.

A structure analogous to CGC(Ind)$ZrCl_2$ was recently reported by Alt,[8b] in which the indenyl ring is replaced by a fluorenyl ring. The two structures are similar in many respects, with CGC(Flu)$ZrCl_2$ having slightly shorter bonding distances for Zr−N (2.034(2) vs 2.041(2) Å), and both Zr−Cl bonds (2.399(1) and 2.397(1) vs 2.429(1) and 2.437(1) Å) as well as longer average distances from Zr to the five bonded carbon atoms of the fluorenyl ligand than to the indenyl ligand (2.523(3) vs 2.505(2) Å). The ligation of the metal center for the fluorenyl structure is slightly more open with a larger bite angle (ipso ring carbon-Si−N angle ≈ 93.5(1)° vs 93.05(10)° for **4**) and a slightly contracted Si−N−Zr angle (104.5(1)° vs 105.88(10)° for **4**). The most striking difference in the two structures is the location of the chlorine atoms. In the less symmetrical indenyl structure, the chlorine ligands are more widely spaced (∠Cl−Zr−Cl = 106.07(3)° in **4** vs 102.9(1)° in CGC(Flu)$ZrCl_2$) and their bisector is rotated 22.1° away from the Zr−Si vector toward the sterically more open side of the CGC(Ind) structure.

V. Ethylene Polymerization Studies. As judged by in situ ^{1}H NMR spectroscopy, bimetallic and monometallic CGC complexes **Zr_2** and **Zr_1** undergo rapid activation with $Ph_3C^+B(C_6F_5)_4^-$ (**B_1**) or bisborate cocatalyst **B_2** in C_6D_6 at room temperature. The metallocenes and cocatalysts react completely within minutes to quantitatively form Ph_3CMe and the active catalysts, which are relatively unstable at room temperature in the absence of ethylene. The resultant active catalysts have significantly greater solubility in 1,2-difluorobezene than do the neutral metallocenes and form clear, light-yellow solutions. Polymerizations with the four combinations of metallocene catalysts and borate cocatalysts illustrated in the catalyst nuclearity matrix (Scheme 2) were carried out under identical conditions at concentrations of 0.05−0.10 mM and were deliberately run to as close to identical conversions (polyethylene yields) as possible (0.75−1.50 h; Table 5a). Procedures were those designed to minimize mass transfer and exotherm effects[14] (see Experimental Section for details). The molecular weights of the product polymers (Table 5a) are modest as expected for such types of CGC Zr catalysts[8,15,16] and this greatly facilitates microstructural characterization by ^{1}H and ^{13}C NMR (see below). GPC-derived polydispersities (polystyrene/polyethylene calibrant) are consistent with single-site polymerization processes (vide infra). As expected for this molecular weight range, the product polymers are somewhat gel-like in toluene rather than precipitating out as solids. It can also be seen that the molecular weights of the product polymers increase to varying degrees with increasing nuclearity of the catalyst−cocatalyst combinations

Table 5. (a) Ethylene Polymerization Data for Metallocenes **Zr_2** and **Zr_1** + Cocatalysts **B_2** and **B_1**[a] and (b) Branches[d] in Polymers Produced by Metallocenes **Zr_2** and **Zr_1** + Cocatalysts **B_2** and **B_1**

(a) Ethylene Polymerization Data

entry no.	catalyst	μmol of cat.	μmol of cocat.	reaction time (h)	polymer yield (g)	activity[b] (x 10^3)	M_n[c] (x 10^2)
1	**Zr_2** + **B_2**	5.0	5.0	1.50	0.94	63 (7)	11
2	**Zr_2** + 2 **B_1**	5.0	10	1.25	1.09	87 (10)	7.6
3	2 **Zr_1** + **B_2**	10	5.0	1.16	1.08	93 (11)	6.3
4	**Zr_1** + **B_1**	10	10	0.75	0.95	127 (15)	6.1

(b) Branches in Polymers

entry no.	catalyst	μmol of cat.	μmol of cocat.	reaction time (h)	ethyl[d] branch	2-ethyl[d] vinylidene end	butyl[d] branch	other[d] branch	2-alkyl[d] vinylidene end
1	**Zr_2** + **B_2**	5.0	5.0	1.50	12 (2)[0.94]	3.4 (4)[0.3]	1.0 (5)[0.1]	3.3 (3)[0.3]	0.4 (2)[0.0 3]
2	**Zr_2** + 2 **B_1**	5.0	10	1.25	2.7 (4)[0.15]	1.0 (3)[0.05]	∼0	2.1 (3)[0.1]	0.5 (2)[0.0 3]
3	2 **Zr_2** + **B_2**	10	5.0	1.16	6.5 (9)[0.29]	1.5 (2)[0.07]	0.6 (3)[0.0 3]	3.6 (3)[0.2]	1.0 (2)[0.0 5]
4	**Zr_1** + **B_1**	10	10	0.75	1.1 (2)[0.05]	0.4 (2)[0.02]	∼0	2.1 (4)[0.1]	0.8 (2)[0.0 4]

[a] Polymerizations carried out on a high vacuum line at 24 °C in 100 mL of toluene under 1 atm of ethylene pressure. [b] Gram polymer/[(mole of cationic metallocene)·atm·h]; estimated uncertainties indicated in parentheses. [c] Calculated from ^{1}H NMR spectra. [d] Units are branches/1000 carbon atoms; estimated uncertainties indicated in parentheses. Quantity in brackets is approximate average branch content/chain. Numbers of branches are calculated from the integration of ^{13}C NMR resonances at chemical shifts of δ 11.26 ppm (CH_3 of ethyl branch), 12.75 ppm (2-ethyl branch), 23.41 ppm (^{n}butyl branch), 36.6 ppm (2-alkyl branch), and 38.21 ppm (CH of longer branches). Branching assignments according to ref 13.

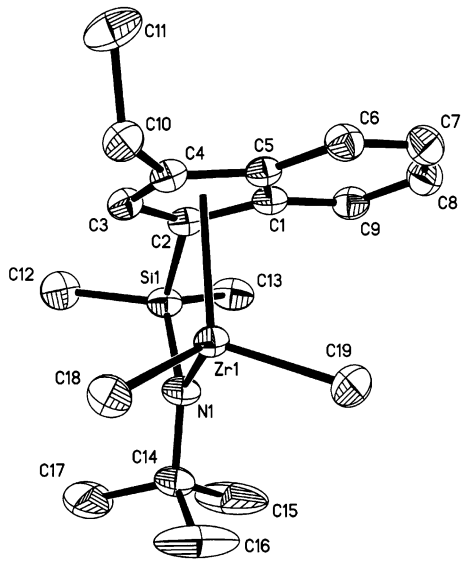

Figure 2. The molecular structure and atom numbering scheme for monometallic indenyl constrained geometry complex [1-Me_2Si(3-Ethylindenyl)(^{t}BuN)]ZrMe_2 (**Zr$_1$**). Thermal ellipsoids are drawn at the 50% probability level. A single enantiomer is shown.

illustrated in the nuclearity matrix (Scheme 2; Table 5a). That of the **Zr$_2$** + **B$_2$** product is nearly 2 times that of the **Zr$_1$** + **B$_1$** product.

^{13}C NMR spectra of the four polyethylene samples of Table 5 are shown in Figure 3 along with assignments for the indicated polymer skeletal positions. Spectral signatures corresponding to isolated branches in linear polyethylenes have been assigned in great detail.[13] As these spectra and the data compiled in Table 5 indicate, branching in the polymer chains is significantly enhanced as the catalyst/cocatalyst nuclearity increases. The combination of bimetallic metallocene and bisborate cocatalyst yields the maximum quantity of branching. The ^{13}C spectra indicate that the most abundant branches in all four polyethylenes are *ethyl branches* [δ 11.26 (CH_3), 26.33 (CH_2), 39.73 (CH)],[13] ranging from ~1.0/chain to ~0.05/chain. There are lesser abundances of ^{n}butyl branches [suggested by the peak at δ 23.41 ($CH_3CH_2CH_2CH_2$CH)][13] and branches having six or more carbon atoms [δ 38.21 (CH), 34.58 (α-CH_2), 27.33 (β-CH_2)].[13] No detectable methyl, ^{n}propyl, or ^{n}pentyl branches, which would be introduced by a macromonomer 2,1-reinsertion process of the type shown in eq 1, can be detected in the ^{13}C spectra of any of the aforementioned polyethylenes, suggesting that branches are introduced mainly by other processes (vide infra). Products arising from the chain epimerization/macromonomer 2,1-reinsertion sequence shown in eq 2, which would introduce methyl branches into the polymer chain, are also below the spectroscopic detection limits.

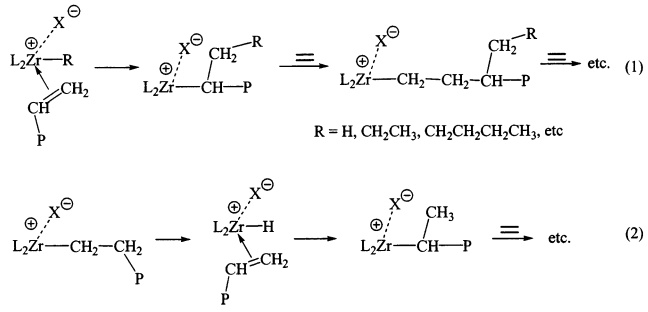

As graphically illustrated in Figure 4, for approximately equal conversions, the product ethyl branch content increases substantially as the catalyst or cocatalyst nuclearity increases. For example, binuclear borate **B$_2$** electrostatically assembles two

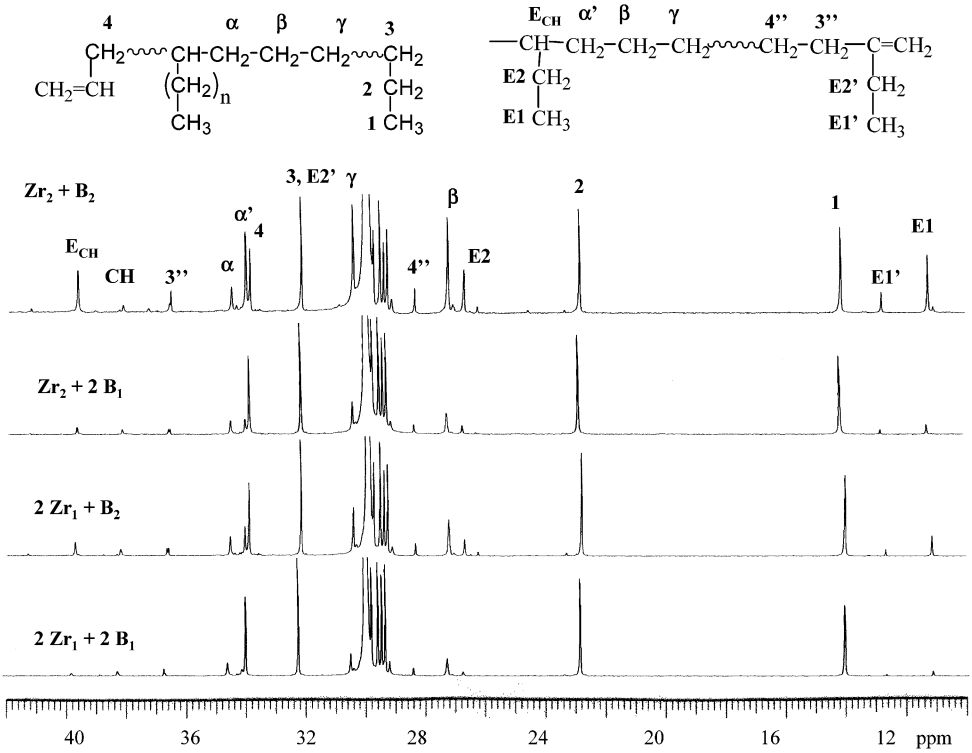

Figure 3. ^{13}C NMR spectra (100 MHz) of polyethylenes (omitting the terminal olefinic end group region) prepared by the catalysts **Zr$_2$** + **B$_2$**, **Zr$_2$** + 2 **B$_1$**, 2 **Zr$_1$** + **B$_2$**, and **Zr$_1$** + **B$_1$** corresponding to the experiments in Table 5. The skeletal labeling scheme and corresponding assignments are also shown.

Scheme 8. Pathways for Ethyl and 2-Ethyl Branch Formation in Ethylene Homopolymerization

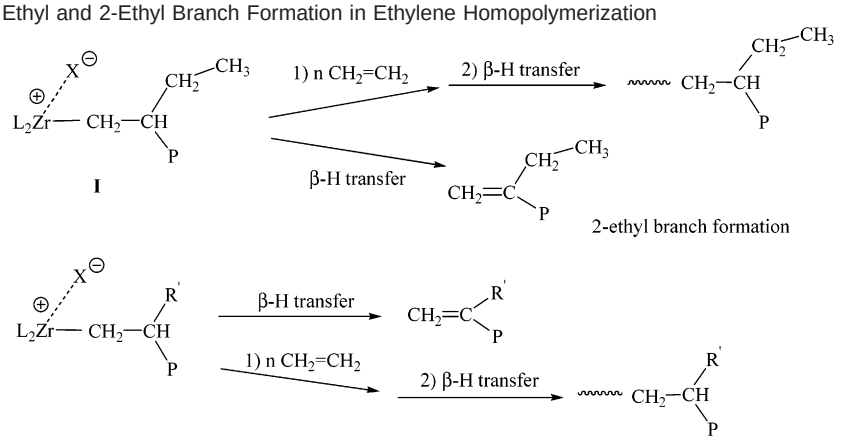

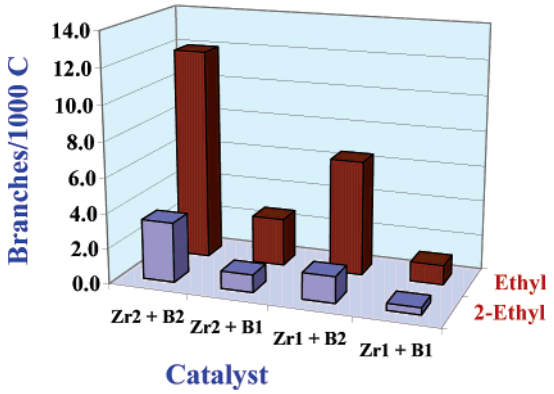

Figure 4. Average number of ethyl and 2-ethyl branches per 1000 C atoms in the polyethylenes prepared in ethylene homopolymerization by the catalysts $\mathbf{Zr_2} + \mathbf{B_2}$, $\mathbf{Zr_2} + \mathbf{B_1}$, $\mathbf{Zr_1} + \mathbf{B_2}$, and $\mathbf{Zr_1} + \mathbf{B_1}$ corresponding to the experiments in Table 5.

monometallic $\mathbf{Zr_1}$ catalyst centers, and the resultant catalyst introduces ~6 times more ethyl branches at the same level of conversion as the same catalyst activated by mononuclear borate $\mathbf{B_1}$. In polymerizations having both bimetallic metallocene catalyst $\mathbf{Zr_2}$ and bifunctional cocatalyst $\mathbf{B_2}$, the active system introduces ≥11 times more ethyl branches per 1000 carbon atoms than does monometallic $\mathbf{Zr_1}$ + monofunctional cocatalyst $\mathbf{B_1}$ at the same level of conversion. This pattern and measured M_n's are catalyst-concentration-invariant over a 5-fold range (Table 7). These data indicate that increased catalyst and cocatalyst nuclearities facilitate the introduction of branching in the polymers. Furthermore, all of the branches contain even numbers of C atoms. Surprisingly, the content of ^{n}butyl branches and other longer branches per 1000 carbon atoms is not increased commensurate with the increased ethyl branching. As indicated in Table 5, the catalytic activities modestly and progressively decrease with increasing catalyst/cocatalyst nuclearity, which is consistent with literature reports on bimetallic metallocene single-site catalyst systems.[6]

^{13}C NMR spectra of the present polyethylenes also indicate the presence of 2-ethyl branches (δ 12.75 (CH_3))[13] and 2-alkyl branches (δ 152 (CH_2=*C*), 108 (*C*H_2=C), 36.6 (CH_2=C-*C*H_2)[13] proximate to vinylidene end groups, which are likewise evident at δ 4.72 (C*H*$_2$=C)[13] in the ^{1}H NMR spectra. These moieties presumably arise via β-H transfer (a priori, either to Zr or to monomer—vide infra)[17,18] within the catalyst structures as shown in Scheme 8. The ratio of 2-ethyl branch to ethyl branch content in each polyethylene sample is similar (ranging from 1:3 to 1:4), suggesting that a catalyst having a local reactive structure of type **I** in Scheme 8 is the common agent in formation of both the ethyl and 2-ethyl branches by sequential CH_2=CH_2 insertion and β-H transfer in all four systems. The selection ratio of β-H transfer to propagation rates in this particular step is then in the range 1:3−1:4. Detailed information on polyethylene chain branching is summarized in Table 5b.

In an effort to differentiate sequential "intermolecular" macromonomer elimination followed by later re-enchainment, branch-forming processes as in Scheme 1, from "intramolecular" multicenter cooperativity effects, studies of product microstructure as a function of conversion time were also undertaken. Extrapolation to zero time/zero conversion should then provide one assay of the "intramolecular" pathway. Table 6 presents time-dependent ethylene polymerization data for monometallic $\mathbf{Zr_1}$ activated by $Ph_3C^+B(C_6F_5)_4^-$ ($\mathbf{B_1}$) for different polymerization reaction times. In the most straightforward scenario, the concentration of any β-H elimination-derived free macromonomers produced during the polymerization process at constant ethylene feed rate (Scheme 1) is expected to increase in the reaction solution during the polymerization and to be enchained (the quantities of such species were at all times below the GC-

(13) (a) Liu, W.; Ray, D. G., III; Rinaldi, P. L. *Macromolecules* **1999**, *32*, 3817−3819. (b) Randall, J. C. *Polymer Characterization by ESR and NMR*; Woodward, A. E., Bovey, F. A., Eds.; ACS Symposium Series 142; American Chemical Society: Washington, DC, 1980; Chapter 6. (c) Axelson, D. E.; Levy, G. C.; Mandelkern, L. *Macromolecules* **1979**, *12*, 41−52.

(14) (a) Li, L.; Marks, T. J. *Organometallics* **1998**, *17*, 3996−4003. (b) Chen, Y.-X.; Metz, M. V.; Li, L.; Stern, C. L.; Marks, T. J. *J. Am. Chem. Soc.* **1998**, *120*, 6287−6305. (c) Yang, X.; Stern, C. L.; Marks, T. J. *J. Am. Chem. Soc.* **1994**, *116*, 10015−10031.

(15) Jia, L.; Yang, X.; Stern, C. L.; Marks, T. J. *Organometallics* **1997**, *16*, 842−857.

(16) Small amounts of a higher molecular weight component (M_w ~ 10 K) are occasionally detected in the GPC. The origin may be catalyst decomposition products.

(17) For discussions of chain transfer mechanisms in single-site propylene polymerization, see (a) Liu, Z.; Somsook, E.; White, C. B.; Rosaaen, K. A.; Landis, C. R. *J. Am. Chem. Soc.* **2001**, *123*, 11193−11207. (b) Lin, S.; Tagge, C. D.; Waymouth, R. M.; Nele, M.; Collins, S.; Pinto J. C. *J. Am. Chem. Soc.* **2000**, *122*, 1127−11285. (c) Resconi, L.; Cavallo, L.; Fait, A.; Piemontesi, F. in ref 1a, p 1253. (d) Coates, G. W. in ref 1a, p 1223. (e) Liu, S.; Tagge, C. D.; Waymouth, R. M.; Nele, M.; Collins, S.; Pinto, J. C. *J. Am. Chem. Soc.* **2000**, *122*, 11275−11285. (f) Veghini, D.; Henling, L. M.; Burkhardt, T. J.; Bercaw, J. E. *J. Am. Chem. Soc.* **1999**, *121*, 564−573. (g) Stehling, U.; Diebold, J.; Kirsten, R.; Röll, W.; Brintzinger, H. H.; Jungling, S.; Mülhaupt, R.; Langhauser, F. *Organometallics* **1994**, *13*, 964−970.

(18) For discussions of chain transfer mechanisms in single-site ethylene polymerization, see (a) Izzo, L.; Riccardis, F. D.; Alfano, C.; Caporaso, L.; Oliva, L. *Macromolecules* **2001**, *34*, 2−4. (b) Wang, L.; Yuan, Y.; Feng, L.; Wang, Y.; Pan, J.; Ge, C.; Ji, B. *Eur. Polym. J.* **2000**, *36*, 851−855. (c) Izzo, L.; Caporaso, L.; Senatore, g.; Oliva, L. *Macromolecules* **1999**, *32*, 6913−6916.

Table 6. (a) Ethylene Polymerization Data for Metallocene $\mathbf{Zr_1}$ + Cocatalyst $\mathbf{B_1}$ as Function of Reaction Time[a] and (b) Branches[f] in Polymers Produced by Metallocene $\mathbf{Zr_1}$ + Cocatalyst $\mathbf{B_1}$ as Function of Reaction Time

(a) Ethylene Polymerization Data

entry no.	catalyst	μmol of cat.	μmol of cocat.	reaction time (h)	polymer yield (g)	activity[b] (x 10^3)	M_n[c] (x 10^2)	M_w[d] (x 10^2)	M_w/M_n[d]
1	$\mathbf{Zr_1 + B_1}$	10	10	0.25	0.35	140 (15)	6.6	7.3	1.1
2	$\mathbf{Zr_1 + B_1}$	10	10	0.75	0.95	127 (15)	6.1	6.7	1.1
3	$\mathbf{Zr_1 + B_1}$	10	10	1.75	2.35	134 (15)	6.8	7.5	1.1
4	$\mathbf{Zr_1 + B_1}$	10	10	3.30	4.50	129 (15)	6.2	7.4	1.2
5[e]	$\mathbf{Zr_1 + B_1}$	10	10	0.033	0.28	170 (20)	6.2	7.4	1.2

(b) Branches in Polymers

entry no.	catalyst	μmol of cat.	μmol of cocat.	reaction time (h)	ethyl[d] branch	2-ethyl[f] vinylidene end	butyl[f] branch	other[f] branch	2-alkyl[f] vinylidene end
1	$\mathbf{Zr_1 + B_1}$	10	10	0.25	0.8(4)	0.2(2)	~0	0.7(2)	0.3(1)
2	$\mathbf{Zr_1 + B_1}$	10	10	0.75	1.1(2)	0.4 (2)	~0	2.1(4)	0.8(2)
3	$\mathbf{Zr_1 + B_1}$	10	10	1.75	2.7(5)	0.6 (3)	1.0(4)	5.7(5)	2.0(4)
4	$\mathbf{Zr_1 + B_1}$	10	10	3.30	4.3(6)	1.1(3)	2.2(3)	6.2(8)	2.7(3)
5[e]	$\mathbf{Zr_1 + B_1}$	10	10	0.033	0.4(2)	0.4(2)	~0	0.4(2)	0.1(1)

[a] Polymerizations carried out on high vacuum line at 24 °C in 100 mL of toluene under 1 atm of ethylene pressure. [b] Gram polymer/[(mole of cationic metallocene)·atm·h]; estimated uncertainties indicated in parentheses. [c] Calculated from ^{1}H NMR spectra. [d] By GPC vs polystyrene/polyethylene standards. Small feature also observed at $M_n \approx 10$ K. [e] Polymerizations carried out on high-pressure line under 5.0 atm of ethylene pressure. [f] Units are branches/1000 carbon atoms; estimated uncertainties indicated in parentheses. Numbers of branches are calculated from the integration of ^{13}C NMR resonances at chemical shifts of δ 11.26 ppm (CH_3 of ethyl branch), 12.75 ppm (2-ethyl branch), 23.41 ppm (^{n}butyl branch), 36.6 ppm (2-alkyl branch), and 38.21 ppm (CH of longer branches). Branching assignments according to ref 13.

Table 7. (a) Ethylene Polymerization Data for Metallocene $\mathbf{Zr_2}$ + Cocatalyst $\mathbf{B_2}$ as Function of Reaction Time[a] (b) Branches[f] in Polymers Produced by Metallocene $\mathbf{Zr_2}$ + Cocatalyst $\mathbf{B_2}$ as Function of Reaction Time

(a) Ethylene Polymerization Data

entry no.	catalyst	μmol of cat.	μmol of cocat.	reaction time (h)	polymer yield (g)	activity[b] (x 10^3)	M_n[c] (x 10^2)	M_w[d] (x 10^2)	M_w/M_n[d]
1	$\mathbf{Zr_2 + B_2}$	5.0	5.0	0.15	0.10	67 (7)	10	12	1.2
2	$\mathbf{Zr_2 + B_2}$	5.0	5.0	0.60	0.48	80 (11)	11	13	1.2
3	$\mathbf{Zr_2 + B_2}$	5.0	5.0	1.50	0.94	63 (7)	11	13	1.2
4	$\mathbf{Zr_2 + B_2}$	5.0	5.0	3.00	2.02	67 (7)	9.5	11	1.2
5	$\mathbf{Zr_2 + B_2}$	5.0	5.0	6.50	4.10	63 (7)	9.4	13	1.4
6[e]	$\mathbf{Zr_2 + B_2}$	5.0	5.0	0.27	2.30	170 (20)	8.8	11	1.2
7	$\mathbf{Zr_2 + B_2}$	25.0	25.0	0.67	2.30	69 (20)	11		

(b) Branches in Polymers

entry no.	catalyst	μmol of cat.	μmol of cocat.	reaction time (h)	ethyl[f] branch	2-ethyl[f] vinylidene end	butyl[f] branch	other[f] branch	2-alkyl[f] vinylidene end
1	$\mathbf{Zr_2 + B_2}$	5.0	5.0	0.15	8.4 (8)	~0	~0	~0	~0
2	$\mathbf{Zr_2 + B_2}$	5.0	5.0	0.60	8.9 (8)	2.5 (5)	~0	1.0 (2)	0.4 (2)
3	$\mathbf{Zr_2 + B_2}$	5.0	5.0	1.50	12 (2)	3.4 (4)	1.0 (5)	3.3 (3)	0.4 (2)
4	$\mathbf{Zr_2 + B_2}$	5.0	5.0	3.00	13 (2)	3.4 (5)	1.0 (2)	4.0 (3)	1.2 (3)
5	$\mathbf{Zr_2 + B_2}$	5.0	5.0	6.50	13 (2)	3.8 (5)	1.1 (3)	4.4 (5)	1.5 (3)
6[e]	$\mathbf{Zr_2 + B_2}$	5.0	5.0	0.27	8.9 (8)	4.1 (5)	~0	1.8 (2)	0.5 (2)
7	$\mathbf{Zr_2 + B_2}$	25.0	25.0	0.67	8.5 (8)	2.2 (5)	~0.6 (3)	3.2 (2)	0.8 (2)

[a] Polymerizations carried out on high vacuum line at 24 °C in 100 mL of toluene under 1 atm of ethylene pressure. [b] Gram polymer/[(mole of cationic metallocene).atm.h]; estimated uncertainties indicated in parentheses. [c] Calculated from 1H NMR spectra. [d] By GPC vs polystyrene/polyethylene standards. Small feature observed at $M_n \approx 10$ K. [e]Polymerizations carried out on high-pressure line under 5.0 atm of ethylene pressure. [f] Units are branches/1000 carbon atoms; estimated uncertainties indicated in parentheses. Numbers of branches are calculated from the integration of ^{13}C NMR resonances at chemical shifts of δ 11.26 ppm (CH3 of ethyl branch), 12.75 ppm (2-ethyl branch), 23.41 ppm (^{n}butyl branch), 36.6 ppm (2-alkyl branch), and 38.21 ppm (CH of longer branches). Branching assignments according to ref 13.

MS detection limits). Not surprisingly, the content of *all types of branches including ethyl, 2-ethyl, ^{n}butyl, 2-alkyl, and other branches increases at longer polymerization times*, presumably because of increased bimolecular capture/reinsertion of these macromonomers (Table 6b). However, the measured product M_w and M_n values remain essentially constant, indicating that the enchainment of these fragments does not greatly alter the number average molecular mass. In regard to ethyl branching, as illustrated in Figure 5A, the average content of ethyl branches/1000C atoms in the 4.50-g polymer sample produced over a 3.30-h $\mathbf{Zr_1 + B_1}$ polymerization time is ~5 times greater than the average ethyl branch content in the 0.35-g polymer sample produced over a 0.25-h polymerization time and is ~4 times greater than the average ethyl branch content in the 0.95-g polymer sample produced over a 0.75-h polymerization time. The relatively constant catalytic activities with time are in accord with good catalyst thermal stability under these conditions, minimal intrusion of mass transfer effects, and approximately constant propagation/chain transfer rate ratios. The ^{13}C NMR spectra of these four polyethylene samples are shown in Figure 1S, and detailed analytical information on branching is summarized in Table 6b.

Table 7 presents contrasting ethylene polymerization data for bimetallic CGC complex $\mathbf{Zr_2}$ activated by the bifunctional cocatalyst $\mathbf{B_2}$ as a function of polymerization conversion time. As can be seen from the table, the catalyst activity and product molecular weight do not change significantly over 6.5-h reaction time, indicating appreciable thermal stability of the catalyst,

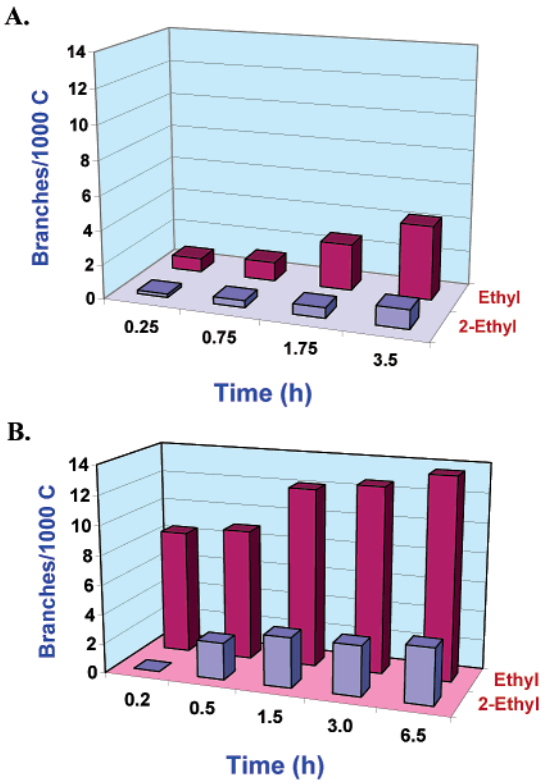

Figure 5. (A) Average number of ethyl and 2-ethyl branches per 1000 C atoms in the polyethylenes prepared in ethylene homopolymerization by the catalyst $\mathbf{Zr_1} + \mathbf{B_1}$ corresponding to the experiments in Table 6. (B) Average number of ethyl and 2-ethyl branches per 1000 C atoms in the polyethylenes prepared in ethylene homopolymerization by the catalyst $\mathbf{Zr_2} + \mathbf{B_2}$ corresponding to the experiments in Table 7.

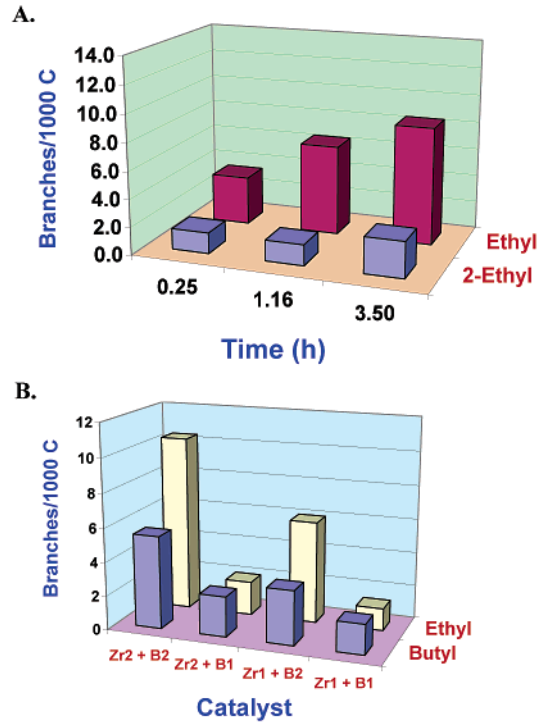

Figure 6. (A) Average number of ethyl and 2-ethyl branches per 1000 C atoms in the polyethylenes prepared in ethylene homopolymerization by the catalyst 2 $\mathbf{Zr_1} + \mathbf{B_2}$ corresponding to the experiments in Table 8. (B) Average number of ethyl and ^{n}butyl branches per 1000 C atoms in the ethylene/1-hexene copolymers prepared in ethylene + 1-hexene copolymerization by the catalysts $\mathbf{Zr_2} + \mathbf{B_2}$, $\mathbf{Zr_2} + \mathbf{B_1}$, $\mathbf{Zr_1} + \mathbf{B_2}$, and $\mathbf{Zr_1} + \mathbf{B_1}$ corresponding to the experiments in Table 9.

minimal mass transfer effects, stable propagation/chain transfer rate ratios, and minimal re-enchainment of large fragments under the present polymerization conditions. Most importantly, as indicated by entry 1 in Table 7b, a significant quantity of ethyl branches (but not other branches—these require longer reaction times) is produced in the $\mathbf{Zr_2} + \mathbf{B_2}$ polymerization system even in the earliest stages of the polymerization. Here, the ethyl branch content of the $\mathbf{Zr_2} + \mathbf{B_2}$-derived product is ~11 times greater than that of the $\mathbf{Zr_1} + \mathbf{B_1}$-derived product. Interestingly, as illustrated in Figure 5B, the average ethyl branch content increases only modestly over the time course of the polymerization reaction and is accompanied by parallel increases in 2-ethyl, ^{n}butyl, 2-alkyl, and longer branch content as well, as seen in the $\mathbf{Zr_1} + \mathbf{B_1}$-mediated polymerizations (vide supra). For ethyl branching, the average branch content in the 4.10-g polymer sample produced over a 6.50-h polymerization reaction time is ~1.54 times greater than the average ethyl branch content in the 0.48-g polymer produced over a 0.60-h polymerization period and ~1.12 times greater than the average ethyl branch content in the 0.94-g polymer produced over a 1.5-h polymerization time. These results indicate that the concentration of macromonomer eliminated and then subsequently re-enchained during the course of the polymerization clearly makes a smaller relative contribution to the total ethyl branch content (but a large contribution to that of other branches) in the high nuclearity case. The ^{13}C NMR spectra of these five polyethylene samples are shown in Figure 2S, and detailed branching content data are summarized in Table 7b. Figures 6A and 3S together with Table 8 summarize the results of similar variable conversion time experiments for catalyst system 2 $\mathbf{Zr_1} + \mathbf{B_2}$. It can be seen here that electrostatically induced CGCZr nuclearity affords significantly higher ethyl branching at zero time than observed with $\mathbf{Zr_1} + \mathbf{B_1}$. Product molecular weight parameters for $\mathbf{Zr_2} + \mathbf{B_2}$ are essentially time-invarient.

To further investigate mechanistic details of the chain transfer processes in these CGC systems, parallel ethylene polymerization experiments under 5.0 atm pressure of ethylene were carried out using similar reaction conditions as shown in the final entries of Tables 6 and 7, respectively. Ethyl branching is still by far the major branch in the polymers. Compared to the polymers produced at 1.0 atm pressure (entry 5, Table 6; entry 6, Table 7), the polymers produced with the $\mathbf{Zr_1} + \mathbf{B_1}$ and $\mathbf{Zr_2} + \mathbf{B_2}$ polymerization systems at 5.0 atm have comparable branching. Importantly, the molecular weights of the polymers produced at 5.0 atm ethylene pressure are nearly identical to those produced at 1.0 atm, implicating chain transfer to monomer as the predominant termination pathway.[17,18,19]

The enhanced polymer ethyl branching observed in the ethylene homopolymerizations mediated by the higher nuclearity catalyst−cocatalyst combinations (especially at lower conversions) suggested, as will be further explored in the Discussion Section, that the polynuclear ion pairs might display an unusual binding/capture affinity for small α-olefin molecules. To further test this hypothesis, ethylene + α-olefin copolymerization

(19) For theoretical studies of single-site chain transfer pathways, see (a) Thorshaug, K.; Stovneng, J. A.; Rytter, E.; Ystenes, M. *Macromolecules* **1998**, *31*, 7149−7165. (b) Klesing, A.; Bettonville, S. *Phys. Chem. Chem. Phys.* **1999**, *1*, 2373−2377. (c) Froese, R. D. J.; Musaev, D. G.; Morokuma, K. *Organometallics* **1999**, *18*, 373−379. (d) Margl, P. M.; Woo, T. K.; Ziegler, T. *Organometallics* **1998**, *17*, 4997−5002.

Table 8. (a) Ethylene Polymerization Data for Metallocene $\mathbf{Zr_1}$ + Cocatalyst $\mathbf{B_2}$ as Function of Reaction Time[a] and (b) Branches[e] in Polymers Produced by Metallocene $\mathbf{Zr_1}$ + Cocatalyst $\mathbf{B_2}$ as Function of Reaction Time

(a) Ethylene Polymerization Data

entry no.	catalyst	μmol of cat.	μmol of cocat.	reaction time (h)	polymer yield (g)	activity[b] (x 10^3)	M_n[c] (x 10^2)	M_w[d] (x 10^2)	M_w/M_n[d]
1	2 $\mathbf{Zr_1} + \mathbf{B_2}$	10	5.0	0.25	0.24	96 (11)	7.2	6.6	1.2
2	2 $\mathbf{Zr_1} + \mathbf{B_2}$	10	5.0	1.16	1.08	93 (11)	6.3	5.7	1.1
3	2 $\mathbf{Zr_1} + \mathbf{B_2}$	10	5.0	3.50	3.20	91 (11)	6.4	6.1	1.2

(b) Branches in Polymers

entry no.	catalyst	μmol of cat.	μmol of cocat.	reaction time (h)	ethyl[e] branch	2-ethyl[e] vinylidene end	butyl[e] branch	other[e] branch	2-alkyl[e] vinylidene end
1	2 $\mathbf{Zr_1} + \mathbf{B_2}$	10	5.0	0.25	3.5 (5)	1.5 (2)	~0	0.4 (1)	~0
2	2 $\mathbf{Zr_1} + \mathbf{B_2}$	10	5.0	1.16	6.5 (9)	1.5 (2)	0.6 (3)	3.6 (3)	1.0 (2)
3	2 $\mathbf{Zr_1} + \mathbf{B_2}$	10	5.0	3.50	8.5 (9)	2.6 (5)	1.8 (3)	4.5 (5)	2.4 (3)

[a] Polymerizations carried out on high vacuum line at 24 °C in 100 mL of toluene under 1 atm of ethylene pressure. [b] Gram polymer/[(mole of cationic metallocene)·atm·h]; estimated uncertainties indicated in parentheses. [c] Calculated from ^{1}H NMR spectra. [d] By GPC vs polystyrene/polyethylene standards. Small feature detected at $M_n \approx 10$ K. [e] Units are branches/1000 carbon atoms; estimated uncertainties indicated in parentheses. Numbers of branches are calculated from the integration of ^{13}C NMR resonances at chemical shifts of δ 11.26 ppm (CH_3 of ethyl branch), 12.75 ppm (2-ethyl branch), 23.41 ppm (^{n}butyl branch), 36.6 ppm (2-alkyl branch), and 38.21 ppm (CH of longer branches). Branching assignments according to ref 13.

Table 9. (a) Ethylene/1-Hexene Copolymerization Data for Metallocenes $\mathbf{Zr_2}$ and $\mathbf{Zr_1}$ + Cocatalysts $\mathbf{B_2}$ and $\mathbf{B_1}$[a] (b) Branches[d] in Polymers Produced by Metallocenes $\mathbf{Zr_2}$ and $\mathbf{Zr_1}$ + Cocatalysts $\mathbf{B_2}$ and $\mathbf{B_1}$

(a) Ethylene Polymerization Data

entry no.	catalyst	μmol of cat.	μmol of cocat.	[hex][a] M	reaction time (h)	polymer yield (g)	activity[b] (x 10^3)	M_n[c] (x 10^2)
1	$\mathbf{Zr_2} + \mathbf{B_2}$	5.0	5.0	0.80	1.25	1.09	87 (9)	11
2	$\mathbf{Zr_2} + 2\ \mathbf{B_1}$	5.0	5.0	0.80	0.75	0.98	131 (13)	8.4
3	2 $\mathbf{Zr_1} + \mathbf{B_2}$	10	10	0.80	0.75	1.00	133 (13)	7.3
4	$\mathbf{Zr_1} + \mathbf{B_1}$	10	10	0.80	0.50	0.96	192 (19)	6.4

(b) Branches in Polymers

entry no.	catalyst	μmol of cat.	μmol of cocat.	[hex][d] M	reaction time (h)	ethyl[d] branch	2-ethyl[d] vinylidene end	butyl[d] branch	other[d] branch	2-alkyl[d] vinylidene end
1	$\mathbf{Zr_2} + \mathbf{B_2}$	5.0	5.0	0.80	1.25	10 (1)	2.7 (3)	5.5 (4)	1.3 (2)	1.1 (2)
2	$\mathbf{Zr_2} + 2\ \mathbf{B_1}$	5.0	5.0	0.80	0.75	2.0 (2)	0.7 (1)	2.4 (3)	0.8 (1)	0.5 (1)
3	2 $\mathbf{Zr_1} + \mathbf{B_2}$	10	10	0.80	0.75	6.0 (5)	2.0 (2)	3.2 (3)	1.7 (2)	1.2 (1)
4	$\mathbf{Zr_1} + \mathbf{B_1}$	10	10	0.80	0.50	1.3 (2)	0.4 (1)	1.8 (2)	1.4 (2)	0.9 (2)

[a] Polymerizations carried out on high vacuum line at 24 °C in 100 mL of toluene under 1 atm of ethylene pressure. [b] Gram polymer/[(mole of cationic metallocene)·atm·h]; estimated uncertainties indicated in parentheses. [c] Calculated from ^{1}H NMR spectra. [d] Units are branches/1000 carbon atoms; estimated uncertainties indicated in parentheses. Numbers of branches are calculated from the integration of ^{13}C NMR resonances at chemical shifts of δ 11.26 ppm (CH_3 of ethyl branch), 12.75 ppm (2-ethyl branch), 23.41 ppm (^{n}butyl branch), 36.6 ppm (2-alkyl branch), and 38.21 ppm (CH of longer branches). Branching assignments according to ref 13.

experiments were conducted in a manner parallel to the above homopolymerizations.

VI. Ethylene + α-Olefin Copolymerization Experiments. Ethylene + 1-hexene copolymerizations with the four combinations of CGC catalysts and borate cocatalysts illustrated in the catalyst nuclearity matrix of Scheme 2 were carried out under identical reation conditions and to essentially identical conversions (see Experimental Section for details). Polymerization data are collected in Table 9. It can be seen that polymerization activities and product molecular weights are only slightly more catalyst/cocatalyst dependent than for the previously discussed ethylene homopolymerizations. For the copolymerizations, activity falls more and molecular weight increases more with increasing catalyst/cocatalyst nuclearity. The 1-hexene incorporation in the polymeric products can be assayed in the ^{13}C NMR by the formation of ^{n}butyl branches.[13] As can be seen from Figure 6B, the catalyst derived from bimetallic complex $\mathbf{Zr_2}$ and bifunctional cocatalyst $\mathbf{B_2}$ incorporates ≥3 times more ^{n}butyl branches than that derived from monometallic $\mathbf{Zr_1}$ and monofunctional cocatalyst $\mathbf{B_1}$. Moreover, by simply using bifunctional cocatalyst $\mathbf{B_2}$ instead of monofunctional cocatalyst $\mathbf{B_1}$, the same metallocene $\mathbf{Zr_1}$ produces polymer with nearly 2 times the quantity of 1-hexene incorporation. The ^{13}C NMR spectra of these four polymer samples are shown in Figure 4S.

Interestingly, the ^{13}C NMR data also reveal that the macromolecules produced in the copolymerization experiments contain similar quantities of ethyl branches as in the aforementioned ethylene homopolymerizations. In other words, ethyl branching in the homopolymer chains is still significantly enhanced as the catalyst/cocatalyst nuclearity is increased, consistent with a model in which enhanced ethyl branch formation is due predominantly to intramolecular binuclear enchainment effects and that this process operates essentially independently of the 1-hexene enchainment. It is reasonable in this scenario that similar quantities of ^{n}butyl branches are introduced by macromonomer reinsertion other than via 1-hexene incorporation.

In an effort to further discriminate between added α-olefin versus possible enchainment processes involving ethylene-derived oligomers, experiments were also carried out with an odd carbon number α-olefin. Thus, ethylene + 1-pentene copolymerizations were carried out under conditions identical to those of the earlier experiments. Polymerization data are summarized in Table 10. The 1-pentene incorporation in the polymer can be assayed by the formation of ^{n}propyl branches

Table 10. Ethylene/1-Pentene Copolymerization Data for Metallocenes $\mathbf{Zr_2}$ and $\mathbf{Zr_1}$, Cocatalysts $\mathbf{B_2}$ and $\mathbf{B_1}$[a]

entry no.	catalyst	μmol of cat.	μmol of cocat.	[P] M	reaction time (h)	polymer yield (g)	activity[b] (x 10^3)	ethyl[d] branch	propyl[d] branch	M_n[c] (x 10^2)
1	$\mathbf{Zr_2} + \mathbf{B_2}$	5.0	5.0	0.80	1.50	1.59	106 (11)	10 (1)	43 (3)	9.5
2	$\mathbf{Zr_2} + 2\,\mathbf{B_1}$	5.0	10	0.80	1.20	1.64	137 (20)	3.5 (2)	16 (1)	5.5
3	$2\,\mathbf{Zr_1} + \mathbf{B_2}$	10	5.0	0.80	1.00	1.51	151 (20)	9.0 (2)	20 (1)	5.1
4	$\mathbf{Zr_1} + \mathbf{B_1}$	10	10	0.80	0.75	1.47	196 (20)	2.0 (2)	11 (1)	6.3

[a] Polymerizations carried out on high vacuum line at 24 °C in 100 mL of toluene under 1 atm of ethylene pressure. [b] Gram polymer/[(mole of cationic metallocene)·atm·h]; estimated uncertainties indicated in parentheses. [c] Calculated from ^{1}H NMR spectra. [d] Units are branches/1000 carbon atoms; estimated uncertainties indicated in parentheses. Numbers of branches are calculated from the integration of ^{13}C NMR resonances at chemical shifts of δ 11.26 ppm (CH_3 of ethyl branch), 12.75 ppm (2-ethyl branch), 23.41 ppm (^{n}butyl branch), 36.6 ppm (2-alkyl branch), and 38.21 ppm (CH of longer branches). Branching assignments according to ref 12.

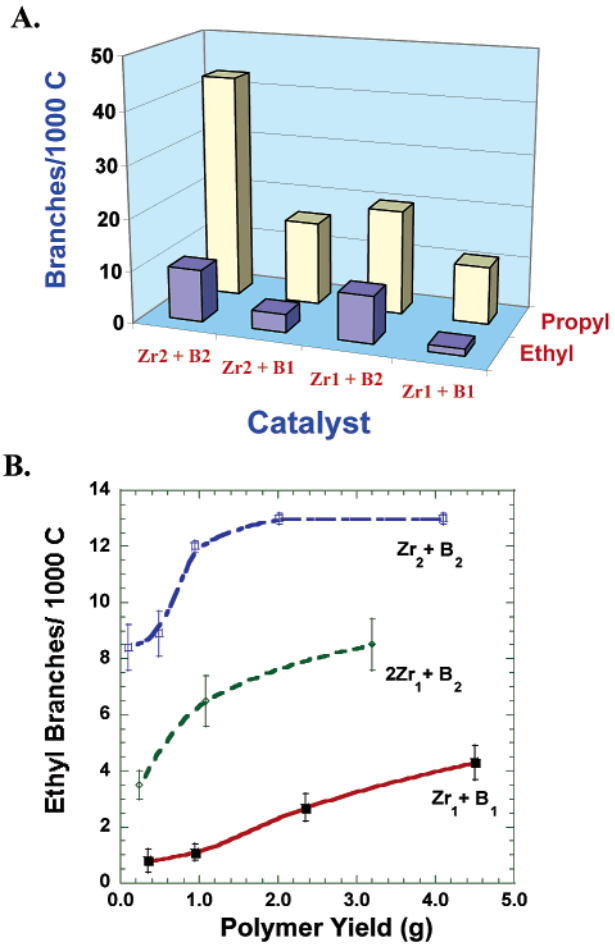

Figure 7. (A) Average number of ethyl and ^{n}propyl branches per 1000 C atoms in the ethylene/1-pentene copolymers prepared in ethylene + 1-pentene copolymerization by the catalysts $\mathbf{Zr_2} + \mathbf{B_2}$, $\mathbf{Zr_2} + \mathbf{B_1}$, $\mathbf{Zr_1} + \mathbf{B_2}$, and $\mathbf{Zr_1} + \mathbf{B_1}$ corresponding to the experiments in Table 10. (B) Comparison of polyethylene ethyl branch evolution with conversion for three catalyst−cocatalyst pairs. Lines through the data points are drawn as a guide to the eye.

[^{13}C chemical shifts at δ 34.51 ($CH_2CH_2CH_3$), 20.33 ($CH_2CH_2CH_3$), 14.66 ($CH_2CH_2CH_3$)],[13] and 2- ^{n}propyl branches [^{13}C chemical shifts at δ 21.32 ($CH_2CH_2CH_3$)].[13] It was demonstrated in the ethylene homopolymerization experiments (vide supra) that negligible ^{n}propyl branches are introduced by macromonomer reinsertion. As can be seen from Table 10 and Figure 7, the catalyst derived from bimetallic $\mathbf{Zr_2}$ and bifunctional $\mathbf{B_2}$ produces ≥4 times more ^{n}propyl branches than that derived from monometallic $\mathbf{Zr_1}$ and monofunctional $\mathbf{B_1}$ (somewhat greater comonomer incorporation than with larger 1-hexene). By using bifunctional cocatalyst $\mathbf{B_2}$ instead of monofunctional cocatalyst $\mathbf{B_1}$, $\mathbf{Zr_1}$ produces polymer with nearly 2 times the amount of 1-pentene incorporation. The ^{13}C NMR spectra of the four polymer samples are shown in Figure 8.

VII. Experiments with Deuterated α-Olefins. In attempting to understand the nature of the enhanced α-olefin binding and enchainment within the polynuclear ion pair structures, the integrity and influence of the substrate C−H bonds was examined via isotopic labeling. This would probe whether C−H bond scission and positional scrambling might occur during the selective enchainment process by the highly electrophilic metal centers or whether α-H agostic (or any other type of agostic)[20] or M−H/C−H equilibria (detectable via significant kinetic[20] or possibly equilibrium isotope[21] effects) might be important. Therefore, ethylene + 1-pentene copolymerization experiments involving competition between a deuterated pentene with the label deliberately chosen to be remote from the double bond (i.e., nonallylic, nonvinylic $CH_2{=}CHCH_2CD_2CD_3$) and 1-pentene were carried out. Ethylene copolymerizations with 1-pentene and 1-pentene-d_5 (1:2.9(1) ratio) were run under identical conditions for both monometallic $\mathbf{Zr_1}$ catalyst + monofunctional cocatalyst $\mathbf{B_1}$ and bimetallic metallocene $\mathbf{Zr_2}$ + bifunctional cocatalyst $\mathbf{B_2}$. The ^{13}C NMR spectra of the two polymer samples are shown in Figure 5S. Because of isotope effects on the chemical shifts, the CD_2 resonances of the $CH_2CD_2CD_3$ branches appear at δ 19.2 ppm (quintet, $^1J_{C-D}$ = 18.7 Hz) in the ^{13}C NMR spectra displaced from δ 20.3 ppm for the corresponding CH_2 in nondeuterated ^{n}propyl branches. The detailed assignments of the chemical shifts are shown in Figure 5S and Table 11. In the copolymer produced by the active catalyst derived from monometallic $\mathbf{Zr_1}$ and monofunctional cocatalyst $\mathbf{B_1}$, the ratio of 1-pentene:1-pentene-d_5 incorporation is 1.00:2.91, yielding a calculated deuterium isotope effect (k_H/k_D) of 1.0(1). Furthermore, the spectra reveal negligible scrambling of the isotopic label over the 1-pentene skeleton or transfer of the label from labeled to unlabeled α-olefin. Such a small isotope effect is consistent with negligible rate-limiting biasing of 1-pentene versus 1-pentene-d_5 enchainment pathways

(20) (a) Prosenc, M. H.; Brintzinger, H. H. *Organometallics* **1997**, *16*, 3889−3894. (b) Grubbs, R. H.; Coates, G. W. *Acc. Chem. Res.* **1996**, *29*, 85−93. (c) Prosenc, M. H.; Janiak, C.; Brintzinger, H. H. *Organometallics* **1992**, *11*, 4036−4041. (d) Cotter, W. D.; Bercaw, J. E. *J. Organomet. Chem.* **1991**, *417*, C1−C6. (e) Krauledat, H.; Brintzinger, H. H. *Angew. Chem., Int. Ed. Engl.* **1990**, *29*, 1412−1413. (f) Piers, W. E.; Bercaw, J. E. *J. Am. Chem. Soc.* **1990**, *112*, 9406−9407. (g) Brookhart, M.; Green, M. L. H.; Wong, L. L. *Prog. Inorg. Chem.* **1988**, *36*, 1−124. (h) Clawson, L.; Soto, J.; Buchwald, S. L.; Steigerwald, M. L.; Grubbs, R. H. *J. Am. Chem. Soc.* **1985**, *107*, 3377−3378.

(21) (a) Slaughter, L. M.; Wolczanski, P. T.; Klinckman, T. R.; Cundari, T. R. *J. Am. Chem. Soc.* **2000**, *122*, 7953−7975. (b) Schroder, D.; Wesendrup, R.; Hertwig, R. H.; Dargel, T. K.; Grauel, H.; Koch, W.; Bender, B. R.; Schwarz, H. *Organometallics* **2000**, *19*, 2608−2615. (c) Bender, B. R. *J. Am. Chem. Soc.* **1995**, *117*, 11239−11246. (d) Hostetler, M. J.; Bergman, R. G. *J. Am. Chem. Soc.* **1992**, *114*, 787−788. (e) Luo, X. L.; Crabtree, R. H. *J. Am. Chem. Soc.* **1990**, *112*, 6912−6918. (f) Calvert, R. B.; Shapley, J. R.; Schultz, A. J.; Williams, J. M.; Suib, G. L.; Stucky, G. D. *J. Am. Chem. Soc.* **1978**, *100*, 6240−6241.

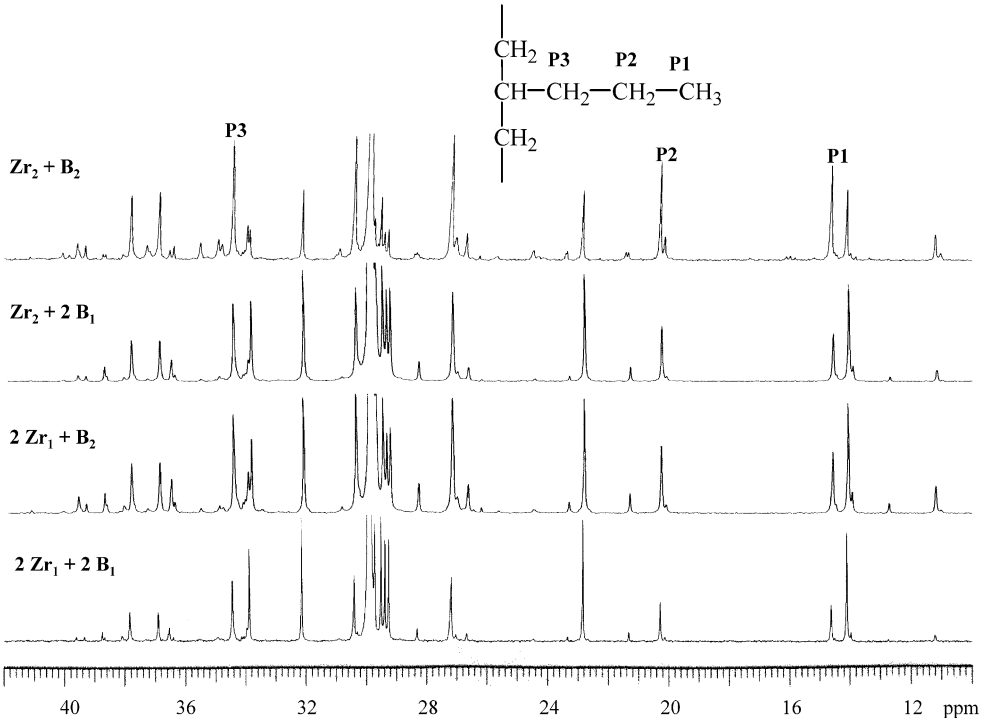

Figure 8. ^{13}C NMR spectra (100 MHz) of ethylene/1-pentene copolymers (omitting the terminal olefinic end group region) prepared in ethylene + 1-pentene copolymerization by the catalysts $\mathbf{Zr_2} + \mathbf{B_2}$, $\mathbf{Zr_2} + 2\ \mathbf{B_1}$, $2\ \mathbf{Zr_1} + \mathbf{B_2}$, and $\mathbf{Zr_1} + \mathbf{B_1}$ corresponding to the experiments in Table 10.

Table 11. Ethylene/[1-Pentene + CH_2=$CHCH_2CD_2CD_3$] Copolymerization Data[a]

entry no.	catalyst	μmol of cat.	μmol of cocat.	[P+P-d_5] M	[P]:[P-d_5]	reaction time (h)	polymer yield (g)	activity[b] (x 10^3)	M_n[c] (x 10^2)
1	$\mathbf{Zr_2} + \mathbf{B_2}$	5.0	5.0	0.53	1:2.9	1.50	1.89	126 (13)	9.7
2	$\mathbf{Zr_1} + \mathbf{B_1}$	10	10	0.53	1:2.9	0.75	1.59	212 (21)	6.6

entry no.	catalyst	μmol of cat.	μmol of cocat.	[P]:[Pd-d_5]	ethyl[d] branch	propyl[d] branch	2-propyl[d] branch	propyl-d_5[d] branch	2-propyl-d_5[d] branch	k_H/k_D
1	$\mathbf{Zr_2} + \mathbf{B_2}$	5.0	5.0	1:2.9 (1)	13 (1)	11 (1)	1.5 (2)	35 (4)	5.5 (6)	0.90 (9)
2	$\mathbf{Zr_1} + \mathbf{B_1}$	10	10	1:2.9 (1)	3.7 (4)	3.3 (3)	0.72 (7)	9.7 (9)	2.0 (2)	1.0 (1)

[a] Polymerizations carried out on high vacuum line at 24 °C in 100 mL of toluene under 1 atm of ethylene pressure, the ratio of 1-pentene and 1-pentene-d_5 is 1:2.9(1). [b] Gram polymer/[(mole of cationic metallocene)·atm·h]; estimated uncertainties indicated in parentheses. [c] Calculated from ^{1}H NMR spectra. [d] Units are branches/1000 carbon atoms; estimated uncertainties indicated in parentheses. Numbers of branches are calculated from the integration of ^{13}C NMR resonances at chemical shifts of δ 11.26 ppm (CH_3 of ethyl branch), 14.63 ppm (CH_3 of ^{n}propyl branch), 20.30 ppm (quintet, 2-$CH_2CD_2CD_3$ and $CH_2CH_2CH_3$), 19.25 ppm (quintet, $CH_2CD_2CD_3$), and 21.32 ppm (2-^{n}propyl branch). Branching assignments according to ref 13.

via agostic or other interactions between the monometallic Zr electrophile and C−H bonds at the 4 and 5 positions of the 1-pentene. In the copolymer produced by the active catalyst derived from bimetallic metallocene $\mathbf{Zr_2}$ + bifunctional cocatalyst $\mathbf{B_2}$, the ratio of incorporation of 1-pentene and 1-pentene-d_5 is 1.00:3.24, yielding a calculated kinetic deuterium isotope effect (k_H/k_D) of 0.90(9). These results show that any C−H/C−D kinetic or equilibrium isotope effects on the enchainment process is at the instrumental detection limits. Additionally, there is no evidence of label scrambling in the product polymer samples. The detailed branching information is summarized in Table 11.

Interestingly, the macromolecules produced in all copolymerization experiments have similar quantities of ethyl branches as in the ethylene homopolymerizations. In other words, ethyl branching in the homopolymer chains is still significantly enhanced as the catalyst/cocatalyst nuclearity increases, which is consistent with the hypothesis that the enhancement in ethyl branch formation is due to intramolecular bimetallic cooperative effects.

Discussion

The present data indicate that as the nuclearity matrix of Scheme 1 is traversed from lower to higher nuclearity, both the extent of low conversion level ethyl branching in the ethylene homopolymer microstructures and the relative rates of α-olefin comonomer enchainment in ethylene + 1-hexene or 1-pentene copolymerizations are substantially enhanced. Concurrently, there is a significant increase in product molecular weight for the highest nuclearity catalyst. The homopolymerization effect to yield enhanced ethyl branching does not require the buildup and subsequent intermolecular re-enchainment of exogenous vinyl-terminated ethylene oligomers, although this process is detectable at longer conversion times. Additionally, catalyst and cocatalyst nuclearity effects on these processes are approximately additive, with the dianion effect being slightly larger (Figures 4−7, 9). The data reveal that the homo- and copolymerization effects operate essentially independently, and significant C−H/C−D kinetic or equilibrium isotope effects on the α-olefin enchainment process are not detectable at sp^3 sites remote from the C=C unsaturation. All catalytic systems evidence increases in other (longer) branch structures as

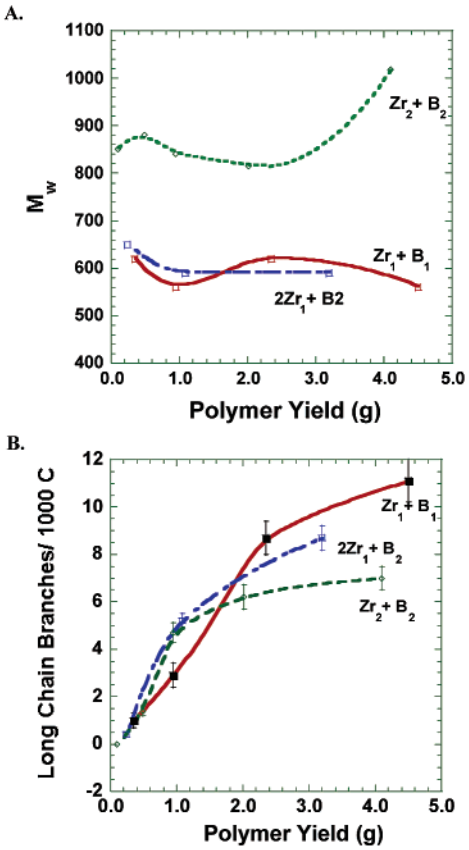

Figure 9. (A) Comparison of polyethylene M_w evolution with conversion for three catalyst−cocatalyst pairs. (B) Comparison of polyethylene C_4 + higher branch evolution with conversion for three catalyst−cocatalyst pairs. Lines through the data points are drawn as a guide to the eye.

conversion proceeds. In the sections below, we discuss the likely origins of these unprecedented catalyst−cocatalyst nuclearity effects.

Chain Transfer Mechanism. β-Hydride transfer from the growing polymer chain directly to coordinated/activated monomer has been reported to be the dominant chain termination process in some ethylene−propylene copolymerizations, as well as some ethylene and propylene homopolymerizations.[16,17,18,20] For the active catalyst derived from bimetallic **Zr$_2$** + bifunctional **B$_2$**, or from monometallic **Zr$_1$** + monofunctional **B$_1$**, the polymers produced at 5.0 atm ethylene pressure have molecular weights experimentally indistinguishable from those produced under the same conditions but at 1.0 atm ethylene pressure (Tables 6a, 7a). This argues that direct β-H transfer from the growing polymer chain to coordinated/activated ethylene predominates (conventional β-H transfer to Zr would increase M_n by ∼5 times), which, as will be seen, is consistent with the observation that most of the excess polyethylene branches are ethyl branches.

II. Nuclearity Effects on Ethylene Polymerization. There are two plausible pathways for the preferential formation of ethyl branches observed in the present study. One pathway is through conventional monometallic macromonomer elimination followed by 1,2 intermolecular reinsertion at an ethyl cation produced by chain transfer to monomer (e.g., Scheme 1 combined with eqs 3 and 4). Izzo et al. recently proposed a mononuclear variant of this type of process for enhanced ethyl branching in *meso*-EBIZrCl$_2$ + MAO-mediated ethylene homopolymerization (the macromonomer is conjectured to remain bound to the cationic metal center at all times although conversion-dependent studies were not reported).[18] There is now ample precedent for d° olefin complexes.[23] A pathway more consistent with the present observations invokes a new type of bimetallic cooperative enchainment process. A plausible scenario is shown in Scheme 9A. Here the eliminated oligomeric or polymeric vinyl mac-

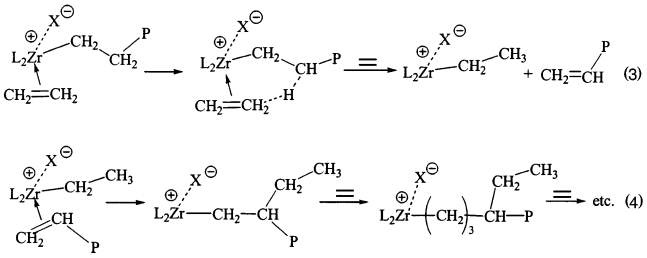

romonomer chain produced at one catalytic center is stabilized by *binuclear interactions* (presumably agostic—the importance of mononuclear examples is of course well-established in cationic d° polymerization systems[20]) involving the adjacent cationic metal center, and the weakly bound oligomeric/polymeric chain therefore has an enhanced probability of subsequent intramolecular re-enchainment with 1,2 regiochemistry at a proximate Zr-ethyl$^+$ or Zr−P$'^+$catalytic site. That the product polyethylene microstructural data indicate that ethyl branch formation is preferred at low conversions over the formation of other longer, even carbon number branches likely reflects the combined predominance of a Zr-ethyl$^+$-forming chain transfer pathway (vs more sterically demanding insertion into the Zr− P$'^+$ bond) combined with favorable intradimer oligomer/polymer insertion versus that of competing ethylene insertion. In addition, a minimally encumbered Zr-ethyl$^+$ group may be more reactive with respect to macromonomer reinsertion and may be stabilized by β-agostic interactions under these conditions. This model is consistent with the general increase in product molecular weight with increasing nuclearity. Another less plausible variant (Scheme 9B) requires that chain transfer to monomer followed by a single ethylene insertion afford a uniquely stable or reactive ^{n}butyl fragment at one Zr$^+$ center. This would then engage in agostic interactions with the second Zr center, and subsequent β-H transfer from the ^{n}butyl chain to Zr results in the formation of a weakly bound 1-butene fragment. An enhanced probability of 1-butene reinsertion (with 1,2 or 2,1 regiochemistry) at the second, proximate Zr center then forms an ethyl branch. In the **Zr$_2$** polymerization system, the data suggest that intramolecular pathways to branched structures are significantly more favorable than intermolecular pathways and that this effect is enhanced in the presence of the binuclear cocatalyst.

(22) Chen, M.-C.; Marks, T. J. *J. Am. Chem. Soc.* **2001**, *123*, 11803−11804.
(23) (a) Carpentier, J.-F.; Maryin, V. P.; Luci, J.; Jordan, R. F. *J. Am. Chem. Soc.* **2001**, *123*, 898−909. (b) Carpentier, J.-F.; Wu, Z.; Lee, W. C.; Strömberg, S.; Christopher, J. N.; Jordan, R. F. *J. Am. Chem. Soc.* **2000**, *122*, 7750−7767. (c) Casey, C. P.; Carpenetti, D. W., II. *Organometallics* **2000**, *20*, 3970−3977. (d) Casey, C. P.; Carpenetti, D. W., II; Sakurai, H. *J. Am. Chem. Soc.* **1999**, *121*, 9483−9484. (e) Abrams, M. B.; Yoder, J. C.; Loeber, C.; Day, M. V.; Bercaw, J. E. *Organometallics* **1999**, *18*, 1389−1401. (f) Galakhov, M. V.; Heinz, G.; Royo, P. *Chem. Commun.* **1998**, 17−18. (g) Casey, C. P.; Fagan, M. A.; Hallenbeck, S. L. *Organometallics* **1998**, *17*, 287−289. (h) Casey, C. P.; Hallenbeck, S. L.; Wright, J. M.; Landis, C. R. *J. Am. Chem. Soc.* **1997**, *119*, 9680−9690. (i) Temme, B.; Karl, J.; Erker, G. *Chem. Eur. J.* **1996**, *2*, 919−924. (j) Casey, C. P.; Hallenbeck, S. L.; Pollock, D. W.; Landis, C. R. *J. Am. Chem. Soc.* **1995**, *117*, 9770−9771. (k)Wu, Z.; Jordan, R. F. *J. Am. Chem. Soc.* **1995**, *117*, 5867−5868.

Scheme 9. Pathways for Ethyl Branch Formation in Ethylene Homopolymerization Mediated by Binuclear Catalysts

A. Macromonomer insertion

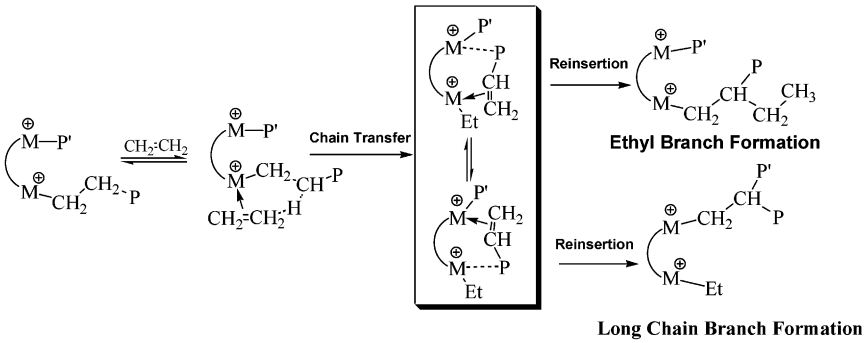

B. 1-Butene elimination/capture

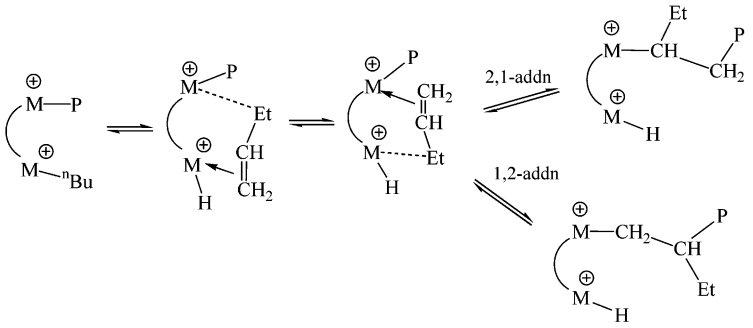

According to Scheme 9A, the ethyl branch content formed via an exclusively intramolecular pathway should be approximately constant over the time course of the polymerization reaction (assuming k(ethylene chain transfer)[ethylene] $\gg$ k(macromonomer chain transfer)[macromonomer]). At the beginning of the polymerization process, any free macromonomer concentration should be low and the ethyl branches introduced (8.4 branches/1000C) would form predominantly via the intramolecular pathway. It is then reasonable to assume that the additional quantities of product ethyl branches (as well as other longer branches) formed after the beginning of the polymerization arise from leakage of chain transfer products from the confines of the polynuclear ion pairs, followed by re-enchainment via a conventional intermolecular reinsertion pathway (Scheme 1). For example, the difference in the ethyl branch content between the 4.10-g polymer sample produced during a 6.50-h $\mathbf{Zr_2} + \mathbf{B_2}$ mediated polymerization reaction (4.6 branches/1000C) and the 0.1-g polymer sample produced during a 0.15-h reaction time (Table 7) should assay approximately the contribution of the intermolecular macromonomer reinsertion pathway, assuming the inter- and intramolecular pathways operate independently. In other words, the average content of ethyl branches in the 4.10-g polymer sample would be ~4.6 branches/1000C if no intramolecular bimetallic capture pathway were operative during the polymerization reaction. Consistent with this scenario, the average content of ethyl branches in the 4.50-g polymer sample produced by monometallic $\mathbf{Zr_1}$ activated by $\mathbf{B_1}$ is ~4.3 branches/1000C (Table 6)—in good agreement with the above estimate. These data are graphically illustrated in Figure 7B. That the product molecular weight is relatively insensitive to conversion (Figure 9A) suggests that the fragments are of relatively low molecular weight or the re-enchainment process is sterically sensitive (supported by the copolymerization experiments—see below).

As noted above, polymer M_n values are virtually insensitive to ethylene pressure. In regard to branching, the data in Tables 6 and 7 suggest that increasing the monomer concentration by 5 times reduces the level of ethyl branching at constant conversion levels by ~30−50% (Table 6 entries 1, 5; Table 7, entries 4, 6). This result cannot be simply explained by enhanced ethylene propagation rates if k(ethylene propagation)[ethylene]/k(ethylene chain transfer)[ethylene] remains essentially constant. Rather, it is plausible that ethylene competition for the polynuclear macromonomer binding site in Scheme 9A competitively introduces ethylene in the "reinsertion" step.

Table 8 presents ethylene polymerization data for monometallic $\mathbf{Zr_1}$ activated by bifunctional $\mathbf{B_2}$ as a function of polymerization reaction time. Again, the catalyst propagation/chain transfer rate ratio is clearly very stable under these polymerization conditions, and there is no evidence of significant mass transfer effects. The average ethyl branch content along with the content of longer branches increase over the course of the polymerization because of the combination of the aforementioned intramolecular bimetallic cooperative effect and intermolecular macromonomer reinsertion (Figures 7B, 9B). Again, the polyethylene molecular weight remains nearly constant (Figure 9A). As can be seen graphically from Figure 6A, both intramolecular bimetallic cooperative and intermolecular macromonomer re-enchainment pathways are important in the formation of ethyl branches in the 2 $\mathbf{Zr_1} + \mathbf{B_2}$ polymerization system. However, because of the presumably looser contact (electrostatic only) between the two catalytic centers, the data suggest that the quantity of ethyl branching introduced via the intramolecular pathway is considerably less

than that introduced by $\mathbf{Zr_2} + \mathbf{B_2}$. The ^{13}C NMR spectra of these three polymer samples are shown in Figure 3S.

As can be seen from Figures 3, 1S, 2S, and 3S, there is negligible methyl, propyl, and pentyl branching observed in the ^{13}C NMR spectra of all the aforementioned ethylene homopolymerization samples. This argues that macromonomer reinsertion in both intra- and intermolecular pathways occurs predominantly via 1,2-regiochemistry, presumably reflecting steric constraints.

The mechanistic scenario advanced here assumes that the catalytically active ion pairs employed behave largely as unaggregated (1:1, 1:2, or 2:1 ion pairs) species. A question has recently been raised on the basis of pulsed gradient spin−echo (PGSE) NMR experiments as to whether metallocene ion pairs might be associated (e.g., as quadruples).[24] Extensive studies of organic electrolytes in low dielectric solvents find that in general, when cations and anions are comparable in dimensions, association is unimportant at solution concentrations below ca. $10^{-4}-10^{-5}$ M.[25] In the present study, catalyst concentrations were maintained in the $5.0 \times 10^{-5}-1.0 \times 10^{-4}$ M range, and for a $\mathbf{Zr_2} + \mathbf{B_2}$ experiment, results were invariant over a 5-fold excursion in concentration (see discussion above; Table 7). In recent work on anion effects in syndiotactic propylene polymerization, which is extremely sensitive to ion pairing, no effects on enchainment stereochemistry were observed over a 31-fold concentration range.[22] In work to be published elsewhere, we show both by cryoscopy and carefully calibrated PGSE NMR studies on a broad series of metallocene ion pairs that most species remain unaggregated even in concentration ranges above those used here.[26]

II. Nuclearity Effects on Ethylene + α-Olefin Copolymerization.

Both the ethylene + 1-hexene and ethylene + 1-pentene copolymerization data indicate that closer contact between two catalytic centers leads to significantly higher extents of comonomer enchainment, with the effect being greater for the smaller α-olefin. As proposed above, it is likely that coordination of α-olefin to a cationic metal center is stabilized by a secondary, possibly agostic interaction with the proximate cationic metal center, which may facilitate/stabilize α-olefin capture/binding at the metal center and enhance the subsequent enchainment probability (Scheme 10). Furthermore, it is possible that the binding of the α-olefin partially blocks/competes for ethylene activation and enchainment sites, explaining the reduced polymerization activity, especially for the higher nuclearity sites. The selectivity between 1-pentene and 1-hexene enchainment helps explain the relative constancy of molecular weights as a function of conversion—larger, sterically more encumbered fragments are not readily re-enchained. As noted above, these processes occur without detectable scrambling of aliphatic C−H bonds at the 4 and 5 positions of deuterium-labeled 1-pentene nor with a statistically significant enchainment kinetic/equilibrium C−H/C−D isotope effect involving these positions.

Scheme 10. Pathways for α-Olefin Enchainment in Binuclear Catalyst Mediated Ethylene Polymerization

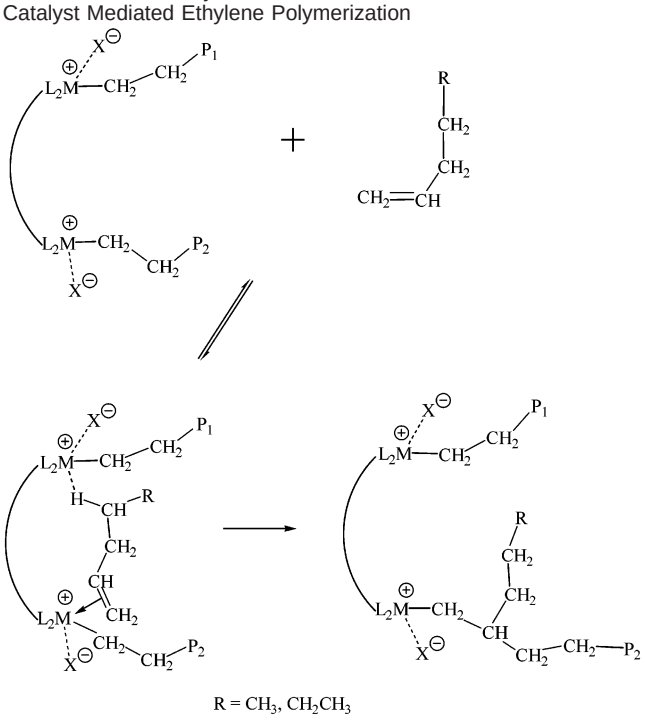

Summary

We have synthesized the binuclear "constrained geometry catalyst" (CGC), (μ-CH_2CH_2-3,3′){(η^5-indenyl)[1- Me_2Si-(^{t}BuN)]($ZrMe_2$)}$_2$ [EBICGC($ZrMe_2$)$_2$; $\mathbf{Zr_2}$] and the trityl bisborate dianion, $(Ph_3C^+)_2$[1,4-$(C_6F_5)_3BC_6F_4B(C_6F_5)_3]^{2-}$ ($\mathbf{B_2}$) to serve as new types of multicenter single-site olefin polymerization catalysts and cocatalysts, respectively. Regarding olefin homopolymerization, increased effective local active site concentrations and bimetallic cooperative effects are observed upon bringing the catalytic centers into close proximity via covalent or electrostatic bonding. Monometallic complex [1-Me_2Si(3-ethylindenyl) (^{t}BuN)]$ZrMe_2$ ($\mathbf{Zr_1}$) was synthesized as a mononuclear control. For ethylene homopolymerization, the branch content of the polyolefin products, primarily ethyl branches, is significantly increased as the catalyst or cocatalyst nuclearity is increased while polymerization activities and product molecular weights vary only modestly (M_n is greatest for $\mathbf{Zr_2} + \mathbf{B_2}$). The predominant ethylene chain transfer pathway in both the $\mathbf{Zr_1} + \mathbf{B_1}$ and $\mathbf{Zr_2} + \mathbf{B_2}$ systems is chain transfer to monomer. Compared to the catalyst derived from monometallic $\mathbf{Zr_1}$ and monofunctional cocatalyst $Ph_3C^+B(C_6F_5)_4^-$ ($\mathbf{B_1}$), the active catalyst derived from bimetallic $\mathbf{Zr_2}$ and bifunctional cocatalyst $\mathbf{B_2}$ introduces ∼11 times more ethyl branches in ethylene homopolymerization. In the $\mathbf{Zr_1} + \mathbf{B_1}$ polymerization system, ethyl (and longer) branches probably arise predominantly via a conventional 1,2 intermolecular reinsertion process involving an ethyl cation. Importantly, however, a heretofore unidentified mutlicenter enchainment pathway is operative in the formation of ethyl branches in the $\mathbf{Zr_2} + \mathbf{B_2}$, $\mathbf{Zr_1} + \mathbf{B_2}$, and $\mathbf{Zr_2} + \mathbf{B_1}$ polymerization systems. Here, macromonomer reinsertion is largely an intradimer process, the data suggesting

(24) (a) Beck, S.; Lieber, S.; Schaper, F.; Geyer, A.; Brintzinger, H.-H. *J. Am. Chem. Soc.* **2001**, *123*, 1483−1489. (b) Beck, S.; Geyer, A.; Brintzinger, H.-H. *Chem. Commun.* **1999**, 2477−2478.
(25) (a) Gordon, J. E. In *The Organic Chemistry of Electrolyte Solutions*; Olah, G. A., Ed.; Interscience Monographs on Organic Chemistry; Wiley: New York, 1975; Chapter 1. (b) Kraus, C. A. *J. Phys. Chem.* **1956**, *60*, 129−141 and references therein. (c) Young, H. S.; Kraus, C. A. *J. Am. Chem. Soc.* **1951**, *73*, 4732−4735. (d) Copenhafer, D. T.; Kraus, C. A. *J. Am. Chem. Soc.* **1951**, *73*, 4557−4561.
(26) Stahl, N.; Marks, T. J., manuscript in preparation.

that the eliminated macromonomer chain produced at one catalytic center is stabilized/detained by bimetallic (presumably agostic) interactions involving the adjacent cationic metal center and that this α-olefin fragment is subsequently enchained in a 1,2 regiochemistry. For ethylene + 1-hexene and ethylene + 1-pentene copolymerizations, α-olefin incorporation is significantly enhanced as catalyst or cocatalyst nuclearity is increased. For example, compared to the catalyst derived from monometallic metallocene **Zr$_1$** and monofunctional cocatalyst $Ph_3C^+B(C_6F_5)_4^-$ (**B$_1$**), the active catalyst derived from bimetallic **Zr$_2$** and bifunctional cocatalyst **B$_2$** introduces ∼3 times more 1-hexene incorporation in ethylene/1-hexene copolymerization and ∼4 times more 1-pentene incorporation in ethylene/1-pentene copolymerization. A mechanism in which the α-olefin comonomer is bound within the multinuclear ion pair in a manner analogous to that is the ethylene homopolymerization and hence has a higher probability of enchainment and is consistent with the data. The results of this study indicate that multinuclear single-site catalysts and cocatalysts can be designed which effect unusual cooperative enchainment processes and hence offer the potential of creating new macromolecular architectures. These possibilities are currently under investigation and results will be reported in due course.[27]

Acknowledgment. The research was supported by the U.S. Department of Energy (olefin polymerization catalysis; Grant DE-FG02-86 ER 13511) and the National Science Foundation (ligand design; Grant CHE-0078998). L.L. thanks Dow Chemical Company for a postdoctoral fellowship. We thank Prof. S. Collins and Dr. G. Abramo for helpful comments.

Supporting Information Available: Experimental section. Figures 1S,2S,3S,4S,5S. Complete X-ray experimental details and tables of bond lengths, angles, and positional parameters for the crystal structures of **1**, **Zr$_1$**, and **4** (PDF). Diagram of high-pressure polymerization reactor. This material is available free of charge via the Internet at http://pubs.acs.org.

JA0201698

(27) (a) Abramo, G. P.; Li, L.; Marks, T. J. *J. Am. Chem. Soc.*, in press. (b) Li, H.; Li, L.; Marks, T. J., manuscript in preparation.